International Journal of *Molecular Sciences*

MDPI

Article

On growth and in growth osseointegration enhancement in PM porous Ti-scaffolds by two different bioactivation strategies: Alkali Thermo-Chemical Treatment and RGD-Peptide coating.

Katrin S. Rappe [1], Monica Ortiz-Hernandez [2,3,4,6], Miquel Punset [2,3,4,5,6], Meritxell Molmeneu [2,3,4,6], Albert Barba [1], Carles Mas-Moruno [2,3,4,6], Jordi Guillem-Marti [2,3,4,6], Cristina Caparrós [2,3,4], Elisa Rupérez [2,3,4,6], José Calero [7], María-Cristina Manzanares [8], Javier Gil [9,10], Jordi Franch [1].

[1] Surgery Department. Veterinary School of Barcelona. Universitat Autònoma de Barcelona, Bellaterra,08193 Barcelona, Spain. Katrin.Rappe@uab.cat, albert.barba@uab.cat, jordi.franch@uab.cat

[2] Biomaterials, Biomechanics and Tissue Engineering Group (BBT), Department of Materials Science and Metallurgical Engineering, Universitat Politècnica de Catalunya (UPC), 08019 Barcelona, Spain. monica.ortiz-hernandez@upc.edu, miquel.punset@upc.edu, meritxell.molmeneu@upc.edu, elisa.ruperez@upc.edu, carles.mas.moruno@upc.edu, jordi.guillem.marti@upc.edu, cristina.caparros@upc.edu.

[3] Barcelona Research Center in Multiscale Science and Engineering, Universitat Politècnica de Catalunya (UPC), 08019 Barcelona, Spain.

[4] Research Centre for Biomedical Engineering (CREB), Universitat Politècnica de Catalunya, 08034, Barcelona, Spain.

[5] UPC Innovation and Technology Center (CIT-UPC), Technical University of Catalonia (UPC), C. Jordi Girona 3-1, 08034 Barcelona, Spain.

[6] Institut de Recerca Sant Joan de Déu (IRSJD), 08034 Barcelona, Spain

[7] AMES GROUP S.A. Carretera Nacional 340, Pol. Ind. "Les Fallulles". 08620 Sant Vicenç dels Horts, Barcelona, Spain. jacalero@ames.es

[8] Human Anatomy and Embryology Unit, Department of Pathology and Experimental Therapeutics, Universitat de Barcelona, L'Hospitalet de Llobregat, 08907 Barcelona, Spain. mcmanzanares@ub.edu

[9] Facultad de Odontología, Campus de Medicina y Ciencias de la Salud, Universidad Internacional de Cataluña (UIC), 08017 Barcelona, Spain. Xavier.gil@uic.es

[10] Bioengineering Institute of Technology. Universitat Internacional de Catalunya. 08195 Sant Cugat del Vallés. Barcelona. Spain.

* Correspondence: Xavier.gil@uic.es

Citation: Lastname, F.; Lastname, F.; Lastname, F. Title. *Int. J. Mol. Sci.* **2022**, *23*, x. https://doi.org/10.3390/xxxxx

Academic Editor: Firstname Lastname

Received: date
Accepted: date
Published: date

Abstract: Lack of primary stability and osteointegration in metallic implants may result in implant loosening and failure. Adding porosity to metallic implants reduces stress shielding effect and improves implant performance allowing the surrounding bone tissue growth inwards the scaffold. However, a bioactive surface is needed to stimulate implant osteointegration and improve mechanical stability. In this study, porous titanium implants were produced by powder sintering to create different porous diameters and open interconnectivity. Two strategies were used to generate a bioactive surface on the metallic foams: an inorganic alkali thermo-chemical treatment and by grafting a cell adhesive tripeptide (RGD). RGD peptides show affinity for integrins expressed by osteoblasts and have been reported to improve osteoblast adhesion, while the thermo-chemical treatment is shown to improve titanium implant osseointegration upon implantation. Bioactivated scaffolds and control samples were implanted in tibiae of rabbits to analyze the effect of these two strategies in vivo regarding bone tissue regeneration through interconnected porosity. Histomorphometric evaluation was performed at 4 and 12 weeks after implantation. Bone index contact (BIC) and bone ingrowth and on-growth were evaluated in different regions of interest (ROIs) inside and outside the implant. The results of this study showed that after long term implantation, the RGD-coated samples presented higher quantification values of quantified newly formed bone tissue in the implants outer area. However, the total analyzed bone in-growth was observed to be slightly greater in the scaffolds treated with alkali thermochemical treatment. These results suggest that both strategies contribute to enhance porous metallic implants stability and osteointegration, and combination of both strategies might be worth pursuing.

Keywords: Ti foams; osseointegration; thermochemical treatment; RGD peptide; in vivo implantation; Histomorphometric evaluation; bone on growth; bone in growth.

1. Introduction

The objective of a wide range of medical and veterinary disciplines for many centuries has been to provide implants with proper functioning and an adequate biological response. Suitable biomechanical properties are sought for bone application biomaterials to stimulate bone tissue growth and consolidation.

According to previous studies, various properties of bone-mimicking biomaterials need to be simultaneously adjusted for optimal bone tissue regeneration and implant osseointegration [1,2]. Cell activity and bone tissue formation are stimulated by several factors such as physical substrate topography, geometrical design, shear stress, stiffness and electrical forces, as well as biochemical elements such as growth factors, genes or proteins [3-6]. Consequently, next-generation tissue engineered scaffolds must integrate a range of biological and physical properties for optimal bone regeneration. It is important that materials possess optimal biocompatibility, osseoconduction and osseointegration properties to achieve rapid implant fixation without causing adverse reactions or rejections [7-9]. Calcium phosphates, bioglass and ceramics have been proven to be biocompatible and have osteoconductive properties through the formation of hydroxyapatite on their surfaces [10]. However, they are biomechanically insufficient as they do not support high stress loads [11-12].

Plain metals, such as titanium, support mechanical loads but do not allow good contact between newly formed bone tissue and implant surface. Therefore, porous titanium implants with open, interconnected macro and micropores were developed to allow bone in-growth penetrating the implant, and bone on-growth over its surface to improve its mechanical interlocking fixation [13-18]. Nowadays, porous titanium and its alloys are commonly used for clinical applications under loading conditions because they permit to adjust its porosity and mechanical features to mimic bone properties for each site of implantation. This enables its use for orthopaedic applications such as fixation screws, spinal fixation devices, artificial ligament anchors, dental implants, or foot and ankle reconstructive Wedges [19-22].

3D open and interconnected pores promote bone-forming cells penetration into the implant and facilitate proper nutrient supply inside a large inner volume for bone ingrowth. Subsequently, cell attachment and proliferation of properly vascularized new bone is achieved, providing a strong and durable implant–bone interaction that enhances the optimal function and the lifetime of the implanted device [17, 23-26].

The scaffold's geometrical external design and its surface macro roughness provide immediate primary mechanical stability to the implant. The high friction forces featured between the rough implant surface and the peri-implant bone tissue increase the implant fixation in its location. Furthermore, metal structure`s porosity reduces the implant's Young's modulus, improving load transfer to adjacent bone tissues. That the risk of implant loosening through mitigation and/or reduction of the deleterious stress shielding related to bone resorption [22, 27-35].

Porous titanium scaffolds can be manufactured using a wide variety of processes [6, 36], such as traditional compression and sintering [16, 27, 37], polymeric sponge replication [38], combustion synthesis [39], powder metallurgy (PM) [16, 26, 40-43], rapid prototyping [36, 40, 44], (SEBM) selective electron beam melting [45-50], (SLM) selective laser melting [15, 43, 51-56], and selective laser sintering [36, 56-57], among the most noteworthy. PM seems to be a particularly advantageous method for manufacturing complex

shapes with interconnected pores without the need of machining steps [16, 42, 58] thus shortening the processing route and decreasing related costs [42, 58-59]. Pores of PM manufactured scaffolds can be created by different modes such as particle arrangement during the first compaction step, use of spacer particles disintegration or by solid-state diffusion during the sintering stage [60]. Moreover, porosity properties such as pore size, total porosity, pore size distribution, porosity gradient and porosity interconnectivity can be optimized using this technique in order to better match the bone mechanical properties [16, 26, 61].

Porous titanium implants alone have been shown to have osseoconductive and osseointegrative properties. However, many treatments are presently available to bioactivate the implants thus improving their properties to accelerate osseointegration. Ti can also undergo a wide range of surface modifications in order to improve cell adhesion, proliferation and differentiation to enhance its osseoconductive and osseointegrative capabilities [6, 30, 62-66]. In this regard, the surface of the porous system can be activated by different functionalizing coatings using calcium phosphates [67-70], demineralized bone matrix [26], (DCB) decellularized bone [25], bone marrow aspirate [71], platelet-rich plasma [72], bone morphogenetic proteins [73-74], mesenchymal stem cells [75-76] and bioactive peptides [77-83].

In this study, highly-interconnected porous Ti scaffolds obtained by PM treated with two different strategies of surface activation have been evaluated. One of the strategies consists of an inorganic thermo-chemical treatment that promotes nucleation and growth of a bone-like apatite layer over the Ti surface [61, 84-86]. The other strategy is a surface coating by grafting of a cell adhesive tripeptide (RGD) [26, 87-90]. RGD peptides show affinity for integrins expressed by osteoblasts, and have been reported to improve osteoblast adhesion and improve implant osseointegration [91-92].

The evaluation of both strategies was performed and compared by means of an in-vivo study using rabbit tibiae as animal model. Highly-interconnected porous Ti scaffolds obtained by PM without treatment were used as control. Two time points were studied in order to evaluate the results at short and long implantation time (4 and 12 weeks).

The results of this study showed that after long time implantation, the peptide-treated samples showed higher values for quantification in the outer area. In the inner area, more variability was observed to the different groups: in terms of total bone ingrowth, it was seen that the scaffolds with the thermochemical treatment showed values slightly above those obtained for the peptide group.

2. Results

2.1. Clinical and radiographic results.

All animals recovered uneventfully from the surgery and no postoperative complications such as foreign body reaction, infection, etc. were observed. During the study, none of the experimental animals had clinical signs of disease, disturbances of gait, or alterations in hematologic or biochemical profiles that could interfere with the study.

Postoperative radiographs showed a proper placement of the titanium implanted cylinders (**¡Error! No se encuentra el origen de la referencia.**). The radiographic evaluation of the isolated tibiae at the end of the study also showed all the titanium cylinders properly placed with no signs of implant migration.

Peri-implant radiolucency was not observed in any sample and good bone-to-implant contact was confirmed radiographically in all the samples indicating an adequate new bone formation response around the implants.

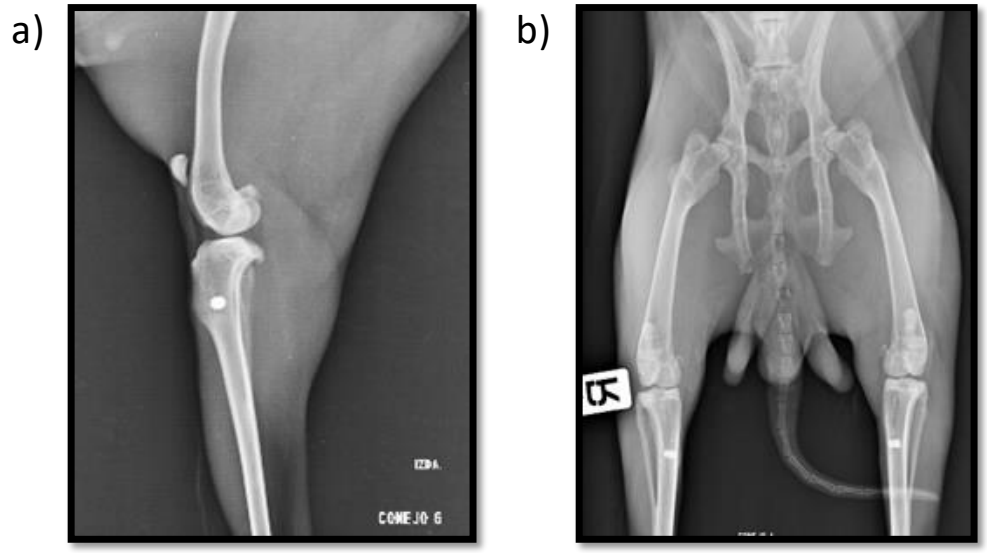

Figure 1: MedioLateral (a) and craniocaudal (b) postoperative X-ray images showing both, insertion point location and implant alignment.

2.2. Porous implant structure and mechanical properties

The porosity of the implants was characterized by mercury immersion porosimetry (MIP) showing an interconnected porosity average of 53% formed by macro and micro pores. The mean diameter for macro pores was 210 μm, while micro pores size ranged from 1 to 15 μm. The bioactivation process of the scaffolds did not modify the values of titanium porosity in terms of interconnectivity. The mechanical properties characterization was previously described elsewhere [26].

2.3. Quantitative histomorphometric evaluation

2.3.1. Postoperative period groups after 4 weeks of implantation

The histomorphometry results are presented as percentage of newly formed bone for every evaluated area designed as "Regions of Interest" (ROIs). A total of 15 samples were obtained after 4 weeks of implantation: 5 from the control group, 5 from the thermochemical group and 5 from the peptide group. All quantitative results for each group are shown in **Table 1**, together with their standard error of the mean (SEM), and graphically represented as shown in (Figure 2).

Table 1: Overall SEM histomorphometric results table in transversal section.

Group of Samples		**BIC**	**OUTER On-growth**	**INNER In-growth**			
Temporal	Treatment	(%)	External (%)	ROI-1 (%)	ROI-2 (%)	ROI-3 (%)	TOTAL (%)
4 Weeks	GC	49.24±10.78	63.64± 7.06	28.18± 7.21	8.34± 2.58	6.33± 1.47	13.48± 3.47
	TCG	56.87± 3.70	64.45± 4.48	34.84± 3.85	13.96± 2.06	6.59± 0.62	18.05± 2.00
	PAG	58.07± 3.60	68.54± 4.40	39.55± 3.75	16.73± 5.34	8.78± 3.98	21.49± 3.67
12 Weeks	GC	59.05± 2.66	67.79± 2.77	43.47± 3.03	8.75± 2.85	10.61± 8.35	20.94± 4.48
	TCG	60.91± 5.93	71.60± 1.93	43.31± 5.58	15.14± 4.49	16.16± 5.62	24.87± 3.39
	PAG	68.93± 4.13	74.55± 4.71	46.03± 5.10	16.41± 5.39	11.53± 5.04	24.66± 4.11

BSE-SEM observation demonstrated that all implant types showed new bone formation inside the pores after 4 weeks of implantation. No adverse tissue reaction or in-

flammatory response was observed in the sections examined. The group of implants functionalized with peptides (PAG) obtained the best results in both outer and inner areas of the implant, showing higher values of Bone on-growth (outside the implant), Bone ingrowth (inside the implant) and BIC than the rest of the Groups. Likewise, the thermochemical-treated group of samples (TCG) revealed superior bone formation values when compared to the control group with no superficial treatment (CG), which showed the lowest values for all ROIs. The differences are statistically significant $p<0.05$.

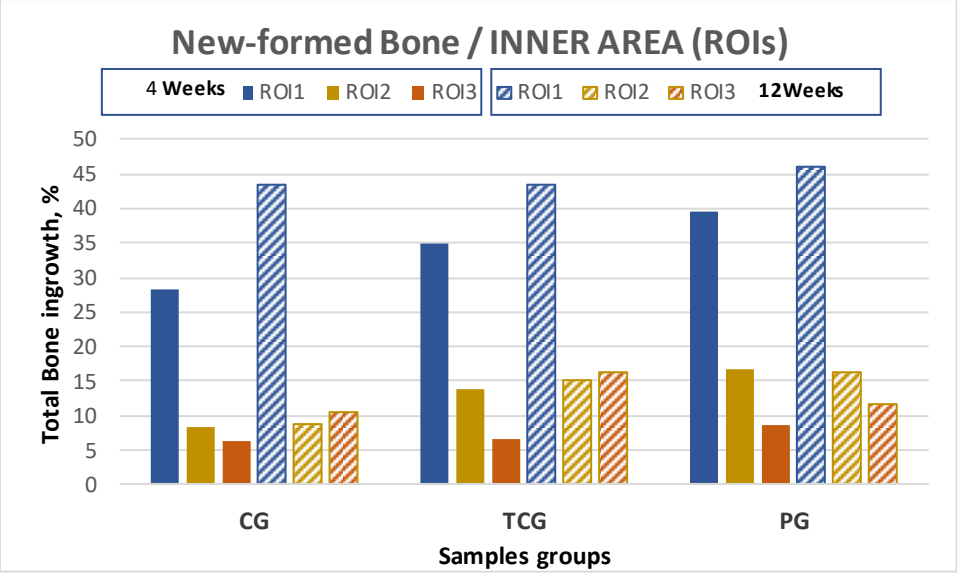

Figure 2. New bone formation in titanium porous foam at 4 and 12 weeks after implantation. (*) means there were no statistically significant differences ($p > 0.05$) depending on the type of samples for all analyzed parameters.

2.3.2. Postoperative period groups after 12 weeks of implantation.

After 12 weeks of implantation, a total of 15 cross-sectional samples were obtained: 5 samples from the control group, 5 samples from the TC and 5 samples from the peptide group. The results obtained for each group in the different areas are displayed in Table 1.

The samples harvested at second time point demonstrated a similar trend as the ones harvested at the first one, with peptide-treated (PAG) samples presenting higher values of bone on-growth in the outer implant area as well as for the BIC.

The results obtained into the evaluated inner ROIs denoted broad variability between the different groups. Thermochemical-treated (TCG) samples showed slightly higher values for the total amount of bone tissues inside the implant than those obtained for the peptide-treated ones. Comparing the different ROIs, the best results for the ROI1 and ROI2 were achieved for the peptide (PAG) group, while the thermochemical-treated samples showed the highest results in ROI3.

The comparative analysis between all samples group results from both time points (4 and 12 weeks) reflected an overall tendency of increase of the newly formed bone percentage along the postoperative period. However, an isolated anomaly was observed in TCG (12 weeks), where the newly formed bone percentage in ROI2 slightly decreased after 12 weeks of implantation (Table 1). The BS-SEM representative micrographs are presented in (Figure 3) revealing differences in both bone in growth and bone on growth as

a function of the group of samples. In Figure 4 is shown the new bone formation in growth after 4 and 12 weeks' implantation.

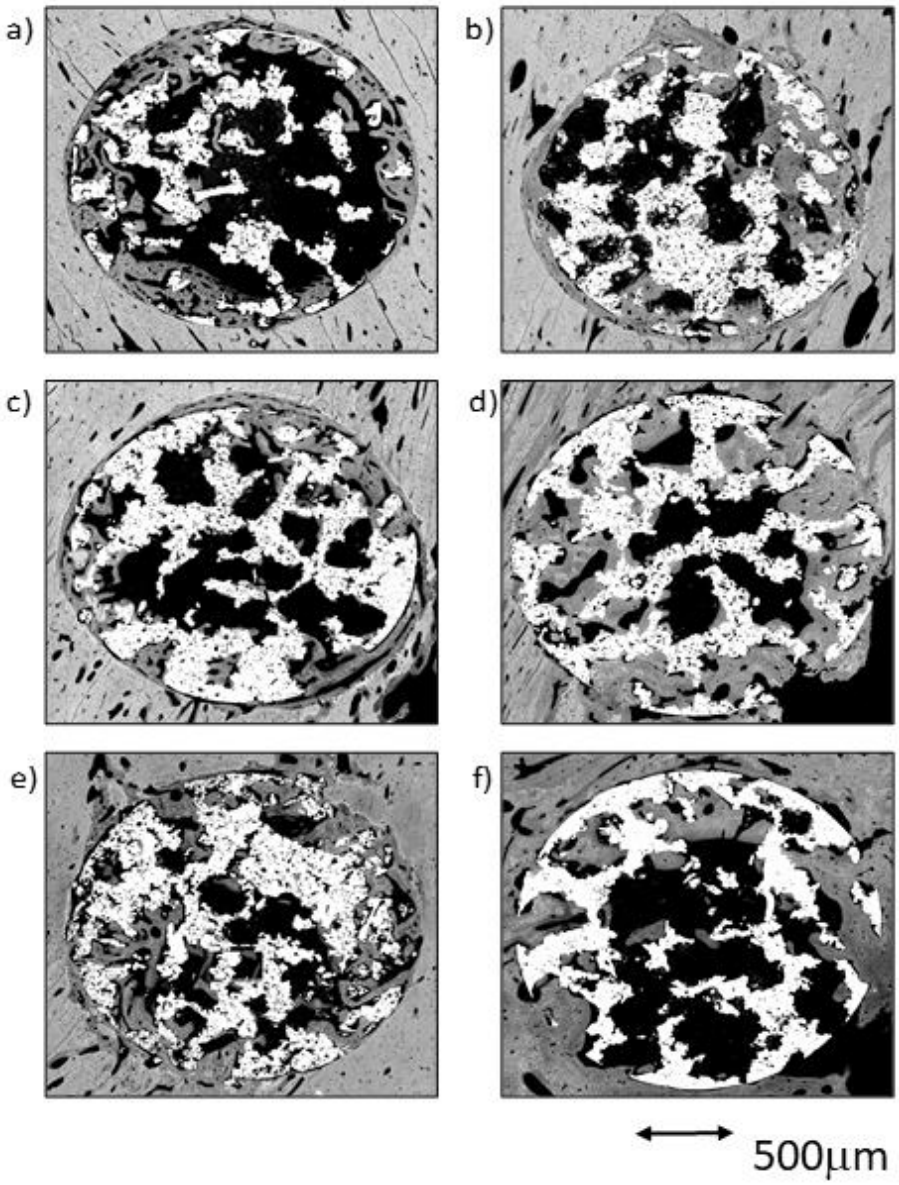

Figure 3. BS-SEM results after 4 weeks (left) and 12 weeks (right) of porous titanium implant insertion in transversal view: (a, b) CG; (c, d) TCG ; (e, f) PAG.

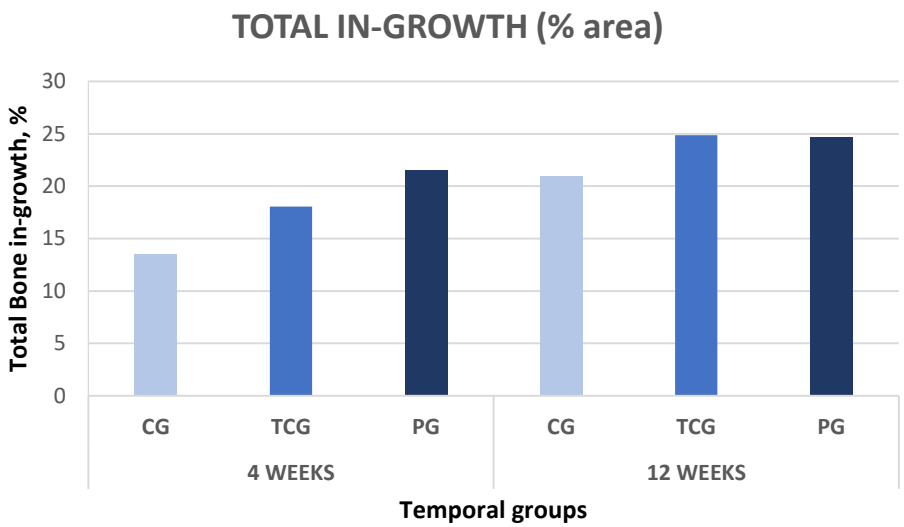

222

223

224 **Figure 4.** Total new bone formation in titanium porous foam 4 and 12 weeks after implantation.

225

226 *2.4. Qualitative evaluation in cross-section view*

227 BSE-SEM high-resolution micrographs were first analyzed in real size in order to ob-
228 tain a global vision. Afterwards, the same images were observed at increased magnifica-
229 tions by 3 independent researchers.

230

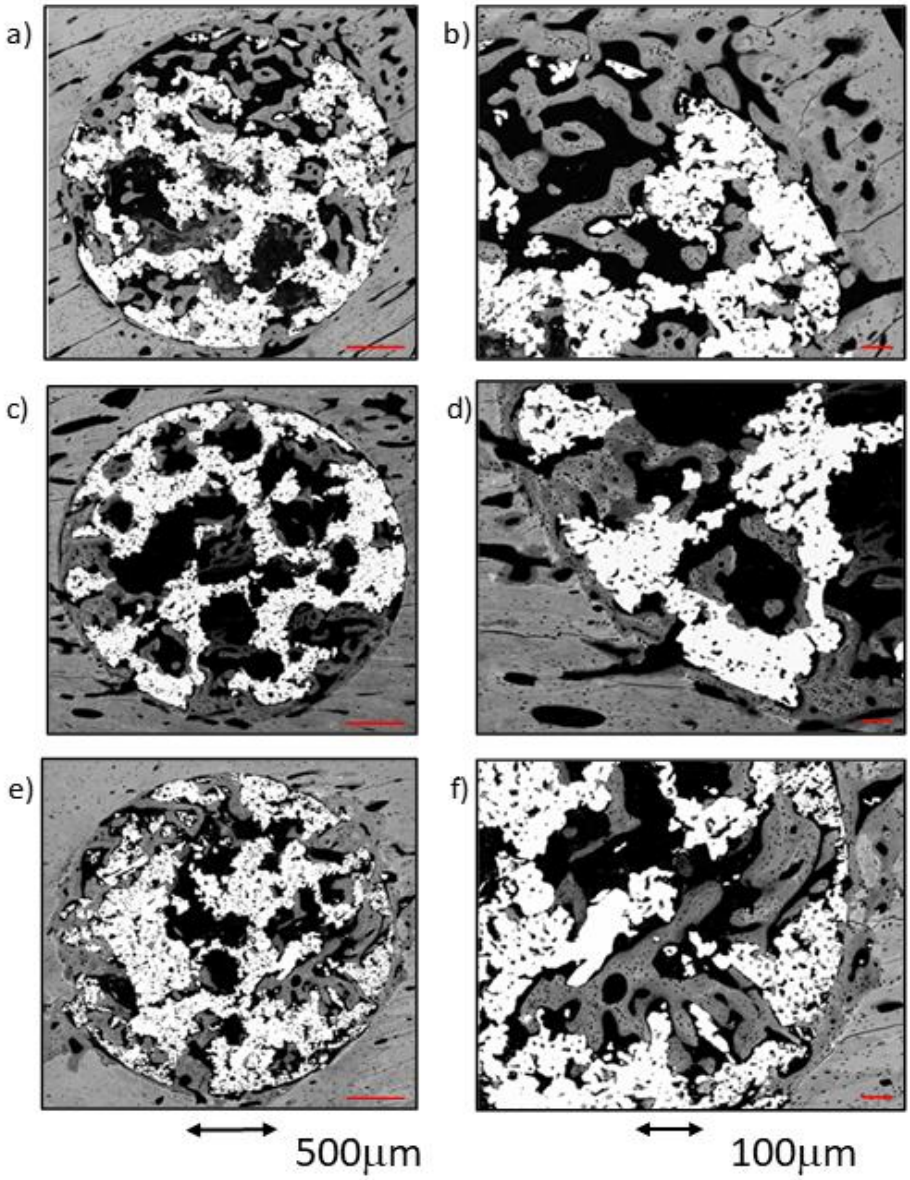

Figure 5. BS-SEM micrographs after 4 weeks of implantation in transversal section view at different magnifications: (a, b) CG; (c, d) TCG; (e, f) PAG

2.4.1. Sample groups after 4 weeks of implantation

CG-group at 4 weeks

In this group, a great difference among the samples was noticed. An almost continuous thin line of newly formed bone tissue was observed in the cortical Outer area for the vast majority of the samples. This bone layer originates in the preexisting cortical bone and is continued by a limited number of trabeculae that penetrate the scaffold's outer area (ROI 1).

The cortical surrounding the implant shows a notable increase in the number and size of the vascular channels, that appear to be continuous with the ones surrounded by the trabeculae invading the scaffold's outer pores. The trabeculae are constituted by an inner core of woven bone surrounded by a reduced number of layers of deposited lamellar bone, and are denser in the ROI1 than in the ROI2. Inside the implants, only a small volume of newly formed bone tissue in the surface of the pores of the central-core of the implant (ROI3) is visible. (Figure 5, a, b)

TCG-group at 4 weeks

As a rule, a notable amount of newly formed bone was noticed in both the external area and inside the implant, coupled with an adequate bone-implant contact (BIC). The cortical surrounding the implant showed evidences of lamellar bone tissue remodeling, continuous with the bone tissues filling the scaffold's peripheral pores (ROI 1). The inner-core regions (ROI 2 and 3) reveal the osseoconductive capacity of the newly-formed bone that covers the outer surface of the scaffold's deeper pores (Figure 5, c and d). The osseous bone tissue that advances towards the center-core of the implant is woven bone, that prevails in the outer area of the samples and establishes an intimate contact with the titanium scaffold inside the porous structure. The lamellar bone remodeling of the scaffold's peripheral pores (ROI 1) is evident by the differences in the shape and orientation of the cell lacunae and in the darker color of the extracellular matrix of the lamellar bone deposited around the vascular channels. The spare remnants of woven bone, lighter in color and with greater cell lacunae, are visible deep within the mass of new bone in the pores Moreover some images suggestive of osteonal remodeling are also visible (Figure 5d), thus proving the maturity of its lamellar components.

PAG-group at 4 weeks

A notable amount of newly formed bone tissue was generally observed in both, outer and inner areas of PAG samples (Figure 5 e and f). The thin, sparse trabeculae visible in the inner area of the scaffolds (ROI3) are thin and are mainly constituted by woven bone, showing a limited contact with the inner micropores of the scaffolds. However, the total amount of newly formed tissue measured by the BIC values appeared to be higher when compared to the other groups. The tissues observed in the outer area of the implants are continuous with the cortical osseous structures; in some samples a thin white line, the cementing line, signaled the initial osteoclastic resorption preceding bone apposition. The dense, well connected newly formed trabeculae are mainly constituted by lamellar bone deposited around what appear as vascular spaces originated in the cortical surrounding the implant. The lamellar bone found between the preexisting cortical and the outer scaffold area (ROI 1) presents some osteonal images.

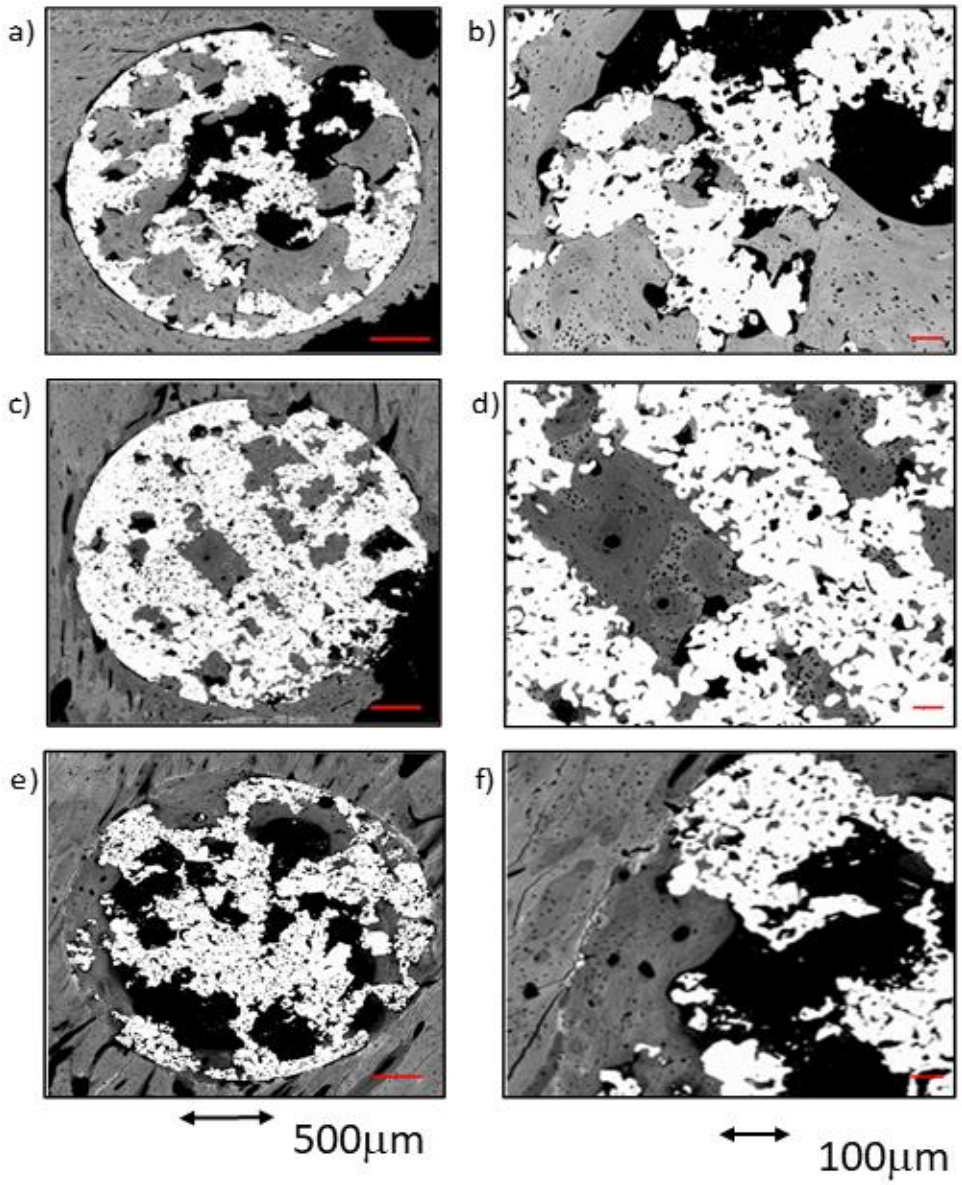

Figure 6. BS-SEM micrographs after 12 weeks of implantation in transversal section view at different magnifications: (a, b) CG; (c, d) TCG; (e, f) PAG.

2.4.2. Sample groups after 12 weeks of implantation

CG-group al 12 weeks

The numerical analysis indicated great variability between samples. In general, a slight increase of the percentage of newly formed bone tissue was seen after 12 weeks of implantation as compared to the same group at 4 weeks. Adequate BIC values were measured at this time point in comparison to 4 weeks. Nevertheless, there was a limited amount of bone tissue inside the central-core (ROI3) and in the inner ring area (ROI2) of the scaffolds. Only in two samples of this group bone tissue was observed reaching the center of the implant.

The newly formed bone tissue observed was mostly found in the ROI1, in form of thick trabeculae in which woven bone scarce remnants are surrounded by lamellar bone.

297 The lamellae are mostly deposited in parallel lines within the scaffold's pores, while some
298 images suggestive of an initial osteonal remodeling are also seen.
299 All CG samples show an intimate and adequate bone-to-metal contact evidenced by the
300 continuity of the remodeling layer around the implant, constituted by lamellar bone. The
301 scaffold's pores are filled up to 60%, mostly found in the ROI1 and ROI2 areas, the inner
302 core of the scaffolds being singularly devoid of bone apposition.
303 The longer implantation time in CG-group of samples resulted in a greater presence
304 of mature bone tissue, along with a higher amount of intimate bone-to-metal contact and
305 micropore filling ratios.
306
307 *TCG-group al 12 weeks*
308 The results analysis reflected great variability between samples in terms of the
309 amount of newly formed bone tissues.
310 One of the samples was found to be almost completely filled with bone tissue, while
311 other two samples presented relatively little bone inside the implant pores. Even so, all
312 implants showed newly formed bone tissue inside ROI3 in a higher amount than the
313 measured at 4 weeks of implantation.
314 The newly formed tissue showed advanced status of maturity in both outer and inner
315 areas of the implants. Very few remnants of woven bone were seen, while lamellar tissue
316 was predominant in the majority of the dense trabecular bone structure that fills both the
317 outer and the inner pores of the scaffolds (Figure 6, c, and d). The presence of osteons in
318 the trabeculae proved its active remodeling. Even in the center of the implants (ROI3),
319 trabeculae are mostly constituted by lamellar tissue. Intimate contact of the newly formed
320 bone tissues within the titanium was observed in most of the samples, inside the titanium
321 macro and micropores. In addition, the newly formed bone tissue appears to spread to-
322 wards the center of the scaffold by taking advantage of the titanium porosity. The increas-
323 ing implantation time in TCG-group resulted in a greater amount of bone tissue with a
324 higher maturity degree.
325 The comparison between TCG and CG groups at 12 weeks reflected a slight superi-
326 ority of the former in terms of tissue maturity, which showed less woven bone tissue in
327 both the outer and inner areas of the implants. Furthermore, TCG showed intimate bone-
328 implant contact in more implant surface than in the CG group.
329
330 *PAG-group al 12 weeks*
331 Compared to the rest of the groups at 12 weeks, the amount of newly formed bone
332 between samples was quite homogeneous in PAG group. Overall, in all samples there was
333 newly formed bone tissue reaching out the center of the implant. The bone-implant con-
334 tact around the entire perimeter of the scaffolds is constituted by lamellar bone, with only
335 scarce remnants of woven bone. Moreover, it should be noticed that this new bone tissue
336 is continuous with the lamellar bone filling the pores of the implant outer area (ROI1) and
337 in the middle area (ROI2). The new formed tissue held high level of maturity in all evalu-
338 ated regions with a general prevalence of lamellar tissue with some osteons and scare
339 evidence of woven bone tissue. Even in the inner core of the implants (ROI3), most of the
340 bone tissue present was lamellar type. The increasing implantation time in PAG-group of
341 samples resulted in improved bone-to metal-contact, even if poor partial contact was re-
342 ported in some areas. New formed tissue seemed to avoid contacting the titanium
343 macropores surface and achieved low penetration rates into the titanium micropores, re-
344 gardless of the implantation time.
345
346 *2.5. Qualitative evaluation in longitudinal view.*

SEM images were firstly analyzed in real size and then observed at increased magnification by three independent researchers.

2.5.1. Sample groups after 4 *weeks of implantation*

CG-group at 4 weeks

In the control group it was seen that the vast majority of the newly formed tissue was continuous with the one found in the cortex. In two of the three samples, bone apposition was observed in connection with the endosteal cortical surface but only some of the samples showed bone growth in connection with the exosteal cortical bone surface. The results found in this section were very similar to those observed in the cross-sectional images of the same group, showing similar tissue maturity level, partial bone-implant contact and acceptable micropore filling. Cementing lines were found separating the preexisting cortical from the remodeling bone. The structure of the newly formed trabeculae was similar to the ones seen in the cross-sectional images: a thin layer of woven bone covered by lamellar bone. Some of these trabeculae connect the endosteous bone formation with the scaffold's pores, both in the cortical sustaining the scaffold and in the contralateral one. Only a small amount of osseous tissue was seen in the central area of the samples (Fig 7 A).

TCG-group at 4 weeks

In the group of scaffolds with thermochemical treatment, newly formed tissue was observed in the center of the implant of all samples. As in the control group, the newly formed tissue in the scaffold's centers was scarce. Likewise, most of the of bone tissue found within the scaffold's pores was continuous with the cortex, while a small amount of bone was continuous with the endosteal remodeling area as well. Also in this group, two out of three samples presented a newly formed bone tissue coming from the periosteum. Figure 7C shows that the periosteal remodeling trabeculae completely covered the outer surface of the scaffold. These trabeculae are relatively thin and separated by ample spaces.

Lamellar tissue predominates in the outer trabeculae upon a small amount of woven bone tissue. In the center of the implant, lamellar tissue occupies most of the scaffold's pores surrounding scarce remnants of clearer woven bone. Figure 7C also shows the intimate contact of the newly formed bone with the implant, through the large filling of the micropores situated nearer to the bone cortical.

PAG-group at 4weeks

The peptide-functionalized samples showed presence of newly formed tissue in the center of the scaffold in the three samples. Thin trabeculae are visible within the scaffold, both in contact with the cortical endosteal and exosteal remodeling and connecting with some points of the scaffold's pores. The trabeculae are mostly constituted by lamellar bone, surrounding very scarce remnants of woven bone, and are separated by large spaces. The trabeculae situated in continuity with the exosteal and all the endosteal remodeling areas -two in the supporting cortical and one in the contralateral cortical- appear more robust than the ones situated in the pores within the scaffold.

Lamellar tissue was also observed in the outer area with minor presence of woven bone tissue. Compared to the other two groups, it appeared to be the one with the most mature newly formed tissue. Likewise, the bone tissue growth could originate from the cortical bone, but also in a lesser degree from the endosteum or even the periosteum. As in the cross-sectional images, poor contact between the newly formed bone and the metal as well as short filling of the micropores were also observed.

399 *2.5.2. Sample groups* after 12 *weeks of implantation*
400
401 *CG-Group at 12 weeks*
402 The images obtained from the control samples of the 12 weeks postoperative period
403 showed very heterogeneous results. In one of the samples, the newly formed bone tissue
404 barely reached the center of the implant while in the sample showed in Figure 9B the
405 remodeling process covered the center of the implant while in contact with both cortical
406 borders. A dense mass of what appears as lamellar bone covers all the exosteal surface of
407 the scaffold, while the scaffold's pores seem to be filled with tissues continuing the endos-
408 teal remodeling. Some very small woven bone remnants are seen within the lamellar bone.
409
410 *TCG-group at 12 weeks*
411 The longitudinal in-growth analysis of TCG samples shows bone growth as thick tra-
412 beculae in contact with the remodeling of the bone cortical, as well as of both the endosteal
413 and the periosteal cortical surfaces. A limited quantity of bone tissue is observed inside
414 the implants, but in all samples it reaches the inner area, corresponding to ROI3. The bone
415 was mostly lamellar tissue in both outer and inner regions of the implants. In addition,
416 many osteons were observed indicating a high degree of remodeling in the surrounding
417 osseous cortical. Again, the newly formed tissues were in direct contact with the metal
418 surfaces, especially inside the implants. The newly formed tissue seemed to take ad-
419 vantage of the metal surfaces to spread towards the inner-core of the scaffolds. In com-
420 parison to CG group at 12 weeks, TCG's new formed tissue expressed higher maturity as
421 well as better bone-to-metal and more micropore's filling rate values.
422
423 *PAG-group at 12 weeks*
424 The longitudinal analysis showed high variability of results between samples. In gen-
425 eral, a small amount of newly formed tissue was observed, but it connected the central
426 core (ROI3) of the implants with the cortical remodeling in all samples. In two samples,
427 this bone longitudinal in-growth came only from the cortex and, in one of them (Figure
428 9F), a discrete amount of osseous growth coming from both the endosteum and the peri-
429 osteum was also observed. The newly formed tissue being mostly lamellar tissue, while
430 almost no areas of woven bone tissue were observed neither outside nor inside the scaf-
431 folds. Again, a little contact between new formed bone and the metal surfaces was ob-
432 served, with only partial filling of the micropores. The new formed tissue showed direct
433 contact with the bone cortical, but not with metallic surfaces, thus filling the inner core of
434 the scaffolds through the open spaces of the interconnected porosity.
435
436 *2.6. Statistical analysis*
437 No statistically significant differences were found between groups. All the obtained
438 values had a p-value ($p > 0.05$). No significant difference was seen neither at the outer area
439 level, nor at the BICs, nor at total newly formed bone, nor by comparing the different ROIs
440 between them. The obtained results are showed in **Table 2** .

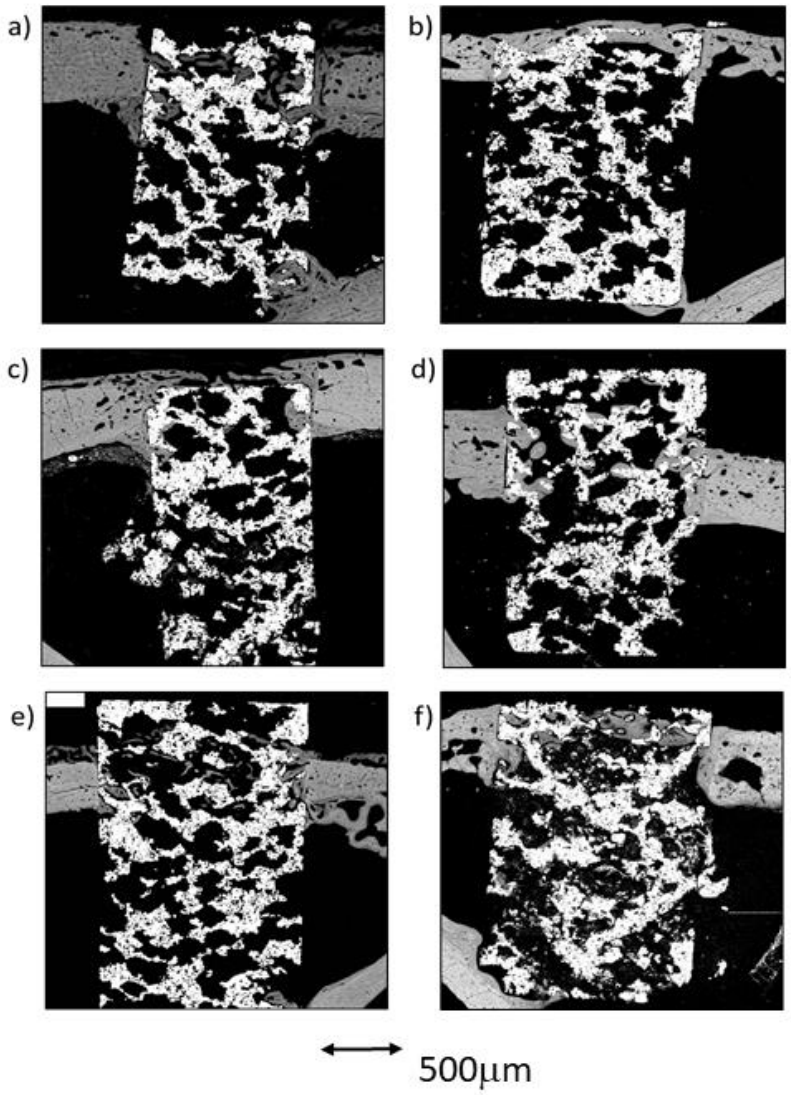

Figure 7. BS-SEM results after 4 weeks (left) and 12 weeks (right) of porous titanium implant insertion in longitudinal section view: (a, b) CG; (c, d) TCG; (e, f) PAG.

Table 2: Overall comparative statistical table of results.

Area	Temporal Groups	Treatment Groups	Significance	p-Value
OUTER AREA	4 WEEKS	CG vs. TCG	NO	0,923
		CG vs. PAG	NO	0,563
		TCG vs. PAG	NO	0,533
	12 WEEKS	CG vs. TCG	NO	0,291
		CG vs. PAG	NO	0,251
		TCG vs. PAG	NO	0,578
INNER AREA	4 WEEKS	CG vs. TCG	NO	0,276
		CG vs. PAG	NO	0,131
		TCG vs. PAG	NO	0,434
	12 WEEKS	CG vs. TCG	NO	0,504
		CG vs. PAG	NO	0,558
		TCG vs. PAG	NO	0,969

BIC	4 WEEKS	CG vs. TCG	NO	0,977
		CG vs. PAG	NO	0,908
		TCG vs. PAG	NO	0,822
	12 WEEKS	CG vs. TCG	NO	0,782
		CG vs. PAG	NO	0,079
		TCG vs. PAG	NO	0,300

3. Discussion

Titanium and its alloys are widely used for various implants in the orthopedic and dental fields due to their good biocompatibility and suitable mechanical properties. However, its elastic modulus is higher than the one of the living bone and, therefore, it may induce bone resorption and stress shielding, following the bone mineralization guidelines that depend on the load distribution described in Wolff's Law according to mechanical stimuli. For this reason, titanium implants with internal and interconnected pores are developed in order to decrease its elastic modulus to the cancellous bone range (around 0.55GPa), as the implants used in this study [93].

The porous titanium implants used in this study were manufactured by sintering using NaCl particles as space holder agent to generate internal and interconnected porosity. These particles were easily removed by washing with distilled water as they are water soluble and allow to obtain a really cheap manufacturing method compared to others such as selective laser fusion [94-95].

According to previous studies, some researchers have observed that the proper porosity for porous titanium implants should range between 25 and 66% [96-97] to stimulate osteointegration. Takemoto et al. in 2005 suggested that porous Ti with 40% of porosity could also be a valid alternative for clinical use [98]. In the present study, the interconnected porous implants presented a total porosity of 53%, enhancing the biological response because of high porosity benefits: it facilitates the transport of body fluids and nutrients; aids the cell propagation inside the implant; and promotes the bone tissue proliferation and maturation into the scaffold structure. However, the balance between porosity rate and mechanical properties is key and must be maintained [99].

The porosity and interconnectivity features are important since they can modify the mechanical properties and the biological performance, as well as the stability and fixation of the implants. The internal interconnection provides tunnels inside the implant that bone cells and extracellular matrix can colonize through and allow neovascularization, thereby enhancing osseointegration and osteoconduction processes [37]. Nonetheless, nowadays there is still some controversy regarding the optimal pore size: when reviewing the published papers, most of the articles mention macropores between 100 and 400 μm as optimal size to enhance osteointegration [20, 100-101]. A reasonable argument to justify these distinct values may be that most of those studies were only focused on the average pore size without considering the pores interconnectivity, which is the communication channel between macropores and a critical factor: macropores with suitable diameter but poor interconnectivity will not permit new bone formation and neovascularization inside the porosity. Channels towards neighbor macropores contribute to keep newly bone tissue ingrowth in optimal conditions [98, 102-104]. In the present study, the porous titanium implants showed an average pore diameter size between 300 and 600 μm, with an average interconnectivity diameter of 210 μm, which allows the implant to be colonized by cells and newly formed bone tissue towards the inner scaffold space.

Although in the vast majority of similar studies samples are analyzed using a single section plane, in this study the samples were evaluated considering two different planes: most of the samples were processed following cross-sections planes, while a smaller

group was processed following longitudinal sections along the major axis of the implants. The main objective of this double plane approach is to obtain the maximum information from the processed implants in order to acquire relevant data on the bone response that takes place inside the implants. By this double approach, a better quantitative assessment of osseointegration and osseoconduction was carried out because the penetration of the newly formed tissue in the innermost areas of the implant was thoroughly analyzed. On the other hand, the longitudinally observed samples allowed a better qualitative evaluation on the topographic origin of the bone tissue (periosteum, cortical, endosteum) and its pattern of propagation into the implant, which was evaluated deeply in detail.

Based on the high-resolution SEM images, an innovative method that allowed automated image evaluation for interconnected porous titanium implants following different ROIs was developed and successfully implemented in this study. In this regard, different implant areas were digitally and automatically defined and subsequently analyzed using ImageJ to calculate the quantity of bone tissue in each ROI and in the bone-implant interface. Up to date, there is no scientific paper available with a detailed protocol to systematically evaluate osseointegration in and on porous titanium implants. The only authors who briefly described their methodology for analyzing porous samples were Takemoto et al. in 2005 [98], who cited the use of Photoshop and ImageJ to determine the bone in growth area rate and the bone affinity index. Based on the information published by Takemoto et al. [98], we designed an automated method that creates different regions of interest using 3 ROIs inside the implant. Likewise, we created the concept of the outer area to define the newly formed bone tissue on the external implant perimeter and we also evaluated the BIC (bone-to-implant contact) to assess the implant fixation by the peripherally newly formed bone in a similar manner than in the method defined by Manresa et al [105]. Using this analysis method, it was observed that all samples from all the groups exhibited newly bone tissue formation inside the implant. In general, the peptide-coated group showed better qualitative and quantitative results compared to the thermochemically treated and control groups in terms of bone ingrowth. However, the samples thermochemically treated revealed a notably higher adhesion between the newly formed bone and the metallic surface (BIC).

In view of the results, the PAG group of samples would have reached slightly higher ingrowth values than the TCG group. However, the TCG group presents BIC values higher than the PAG group in the internal areas of the implant, which would ensure a greater fixation of the implant, as well as a greater and more efficient mechanical bone-to-implant transduction. The greater contact between the newly formed tissue and the internal and external surfaces of the TCG implant would ensure a greater transmission of mechanical loads to the bone, generating lower levels of stress shielding to the bone and, consequently, lower values of bone long-term resorption.

Both types of treatments have efficiently stimulated the growth of newly formed bone tissue, both on the external surface of the scaffold and towards its inner porous structural core, even causing tissue ingrowth from the cortical, periosteal and endosteal bone tissue, in some cases.

It has been reported in many scientific papers, both in vitro and in vivo studies, that porous titanium by itself, without any treatment, has osseoconductive and osseointegrative properties [20, 93-94, 106]. In this study, after 4 weeks of implantation, the presence of woven bone tissue was observed, together with lamellar bone tissue in some areas of the samples from the control group both within micro and macropores. After 12 weeks, the results showed more mature newly formed bone tissue growing towards the inner areas of the scaffolds, with predominant presence of lamellar bone tissue.

Even so, better results were obtained with the thermochemically treated group compared to the control group in terms of ingrowth and new formed bone in the outer area.

There are many scientific articles with thermochemical treatments performed for porous titanium surfaces because it is an inexpensive and simple process. Briefly, when the implant is immersed in NaOH solution, it spreads over all the irregular implant structure achieving a homogeneous bioactive surface, both on the outer part of the implant and in the innermost pores. Furthermore, the thermochemical treatment does not reduce the pore space available for bone tissue growth since it only produces a thin coating of 500 nm-needle-like sodium titanate structures in the surface of the pores, reducing them by a maximum of 1 μm [107] in diameter. The thermochemical treatment induces the formation of a dense and uniform apatite layer in contact with body fluids by ion exchange which is similar to the bone mineral phase. Then, thermochemically treated implants are attached to living bone through this apatite layer providing not only the strong bonding of the apatite layer to bone tissue, but also a uniform gradient of stress transfer from bone to implants [108]. Numerous in vitro studies carried out during the last decades have demonstrated the formation of this apatite layer on the implant surfaces [108-110]. Also several in vivo studies proving the notable effectiveness of thermochemical treatments to improve osseointegration and osseoconduction have been reported [66, 98, 111]. In the present study, TCG implants presented an increased growth of newly formed bone tissue, more mature bone tissue and higher intimate contact and BIC values between bone and implant when compared to CG samples. These results can be attributed to the homogeneous distribution of the treatment, covering all the sample's macro and micropores.

Very little scientific papers have been published measuring bone formation on growth and in growth and the intimate contact of the bone tissue with the metallic surfaces of the macro and micropores. This fact has made difficult to compare our results with other author's reports.

The peptide-coating group showed the best results in terms of newly formed bone tissue quantity and maturity. The aim of peptide bioactivation is to immobilize certain peptide sequences into implant surfaces to induce a specific cellular response, that is, to control the tissue-implant interface through the organic components of bone. This is accomplished through a group of cellular receptors called integrins that are involved in cellular adhesion by extracellular matrix proteins. Integrins interact with short amino acid sequences, in particular with the Arg-Gly-Asp (RGD) sequence, which has been identified as a cellular adhesion mediator for plasma and extracellular matrix proteins [112]. Of the 24 known integrins, 8 subtypes recognize and bind to the RGD sequence. Three of these 8 subtypes are present in osteoblasts, so these sequences are used to promote the adhesion of osteoblasts to implants and thus improve osseointegration [112].

Therefore, peptides attached to implant surfaces have been demonstrated to improve cellular interaction with biomaterials [113]. The first studies dedicated to study the effect of peptides attached to surfaces to bind osteoblasts began in the mid-1990s and the first in vivo study with peptides was carried out in 1999 by Fernández et al. [6]. Nevertheless, there are very few published studies to assess osseoconduction and osseointegration of porous titanium implants using peptides.

After an intensive literature search, no similar study was found to compare the obtained data properly. However, this provides an innovative value to the present study: it reports the first results of an in vivo study with porous titanium samples functionalized with a linear RGD peptide after 12 weeks of implantation. In this study, the excellent performance of bioactive peptide treatments increasing cell adhesion and proliferation, as well as for bone regeneration after long period of implantation time (12 weeks) is confirmed. Unfortunately, no reviewed study gives details on newly formed bone quantity, ingrowth depth, or tissue quality in different time groups as we did in this study. No reference according to the finding observed in this study related to the intimate adherence

of the newly formed bone tissue to the internal macro and micropores of the scaffolds was found either.

As a conclusion, both quantitative and qualitative analyses attained the best results for the samples biofunctionalized with RGD peptide, showing the highest rate of newly formed bone tissue, maturation and bone ingrowth. However, a diminished intimate bone-implant contact inside the samples was also observed. This observation may suggest some extent of peptide degradation or incomplete functionalization in the inner parts of the implant. On the other hand, the peptides may be better available on the outer surface. Thus, superficially, biologically active peptides stimulate bone tissue to grow and penetrate inside macro and micropores, but in-depth, fail to support an intimate adherence of bone to the metallic surface. This hypothesis would justify the good BIC values in the outer area of the implant and the great maturity and amount of new-formed bone tissue at the periphery of the samples, as well as the scarce contact of the newly formed bone inside the implant.

In general, peptides are susceptible to enzymatic degradation by proteases, especially linear peptides, as they are more unstable in nature. A soluble linear peptide is degraded very quickly, however, when anchored to a surface, there is a steric hindrance for enzymes and therefore degradation is slower. A priori, it could be expected that the peptide on the outer side would degrade more rapidly than the one on the inner side, since it is more exposed to the medium. In this case, however, there may be a more rapid cellular adhesion on the outer area which is directly in contact with bone tissue. This interaction is favored by the presence of tailor-made spacing units in the peptide sequence, which ensure its accessibility to the cells. It must also be assumed that the amount of RGD peptides is not the same within the entire implant, since silanization (the method used to bind the peptide to the metal) will be more efficient in the outer area than in the inner part.

If the two bioactivation mechanisms are compared, it can be seen that the two seem to stimulate osseointegration to a certain extent, although it could not be demonstrated with statistically significant differences. The mechanisms of action of an inorganic treatment such as thermochemical treatment compared to an organic one, such as peptide coating, are very different. The inorganic treatment promotes the nucleation of apatite crystals that will be translated into "direct" bone formation, that is, the mineral part of the bone precipitates directly onto the implant. This is associated with bone growth from the implant outwards. In the case of peptides, RGD stimulates the integrins which promote adhesion, mechanotransduction, and finally differentiation and mineralization. Therefore, we could consider it as an indirect mechanism.

Regarding the longitudinal section reviewing the bibliography, we did not find any article describing the origin of the newly formed tissue, that is, if it grows from the cortical, the periosteum or the endosteum. We believe that it is an important aspect since it can indicate a better or worse fixation of the implant. If we only have growth of the bone tissue towards the interior of the implants coming from the periosteum and/or the endosteum, we can deduce that the implant does not fix in the same way as it would with growth coming from the cortical. It would be then necessary a large periosteal and endosteal bridge to minimally stabilize the implant, and these bridges can interfere decisively with the clinical objective of the implant.

4. Materials and Methods

4.1. Implanted materials

The samples used in this study consisted of porous titanium cylindrical implants 6 mm long and 3.5 mm diameter with open and interconnected porosity.

The scaffolds were produced by Pulvi-Metallurgy (PM) technique by mixing grade 2 pure titanium (CP) particles, with an average mean grain size of about 80 μm, with NaCl

particles ranging from 300 μm to 600 μm of diameter as a space holder, in a 65% volume ratio. The manufacturing process was previously described [26].

Three different implant groups were generated according to its surface bioactivation method:

- Bioactivated porous titanium samples by thermo-chemical treatment (TCG).
- Bioactivated porous titanium samples by peptide adsorption (PAG).
- Porous titanium samples with no treatment used as control (CG).

4.2. Surface Bioactivation

Two groups of samples were subjected to surface bioactivation by two different methods: one group by thermo-chemical treatment (TCG) and the other one by peptide adsorption (PAG). The thermo-chemical procedure was performed by 5M NaOH immersion at 60 °C for 24h, followed by drying at 60 °C 24 h and finally heat treated at 600 °C for 1h. This treatment enhances calcium phosphate precipitation over the implant surface in the contact with body fluid.

The peptide adsorption procedure was achieved using covalent grafting of an RGD peptide on the scaffold surface by means of silanization, as previously described [26]. With more detail, the peptide is comprised of the cell-binding sequence Gly-Arg-Gly-Asp-Ser (GRGDS), three units of 6-aminohexanoic acid (Ahx) as spacer [87], and 3-mercaptopropionic acid (MPA), which provides a thiol group as anchoring moiety to react with the silane layer.

4.3. In Vivo Experimentation

All animal procedures in this study were performed in compliance with the Guide for Care and Use of Laboratory Animals (National Research Council, in: Guide for the Care and Use of Laboratory Animals, National Academy Press, Washington, DC, 1996, pp. 41–194) and the European Community Guidelines for the protection of animals used for scientific purposes (Directive 2010/63/EU of the European Parliament and of the Council of 22 September 2010 on the Protection of Animals Used for Scientific Purposes), and under the permission of the National Committee on Human and Animal Research (ref# UAB-CEAAH 2016).

The surgical procedure was performed under standard sterile conditions. Implanted materials were sterilized by gamma radiation at 7 KGy before surgery. The in vivo study was carried out in eighteen female adult New Zealand White (NZW) rabbits (Charles River, France), with an average body weight ranging from 4.0 kg to 6.0 kg.

The experimental animals were randomly divided in two groups: Group A (4 weeks of postoperative period) and Group B (12 weeks of postoperative period), with 9 rabbits for each group. The three implants groups (TCG, PAG, CG) were randomly distributed placing one sample per tibia.

4.4. Surgical Technique

The experimental animals were in optimal physical conditions and were acclimatized individually for 2 weeks prior to surgery. Health status was determined by physical and orthopedic examination, radiographic examination of the rear limbs and results of hematologic and serum biochemical profiles.

For surgical procedure, the animals were preanesthetized using buprenorphine (0.03mg/kg s.c.), midazolam (0.50 mg/kg s.c.) and medetomidine (0.05 mg/kg s.c.). Anesthesia was induced with propofol (2.5mg/kg/s.c.) and then maintained inhaled isoflurane (2%) in an oxygen carrier by mask.

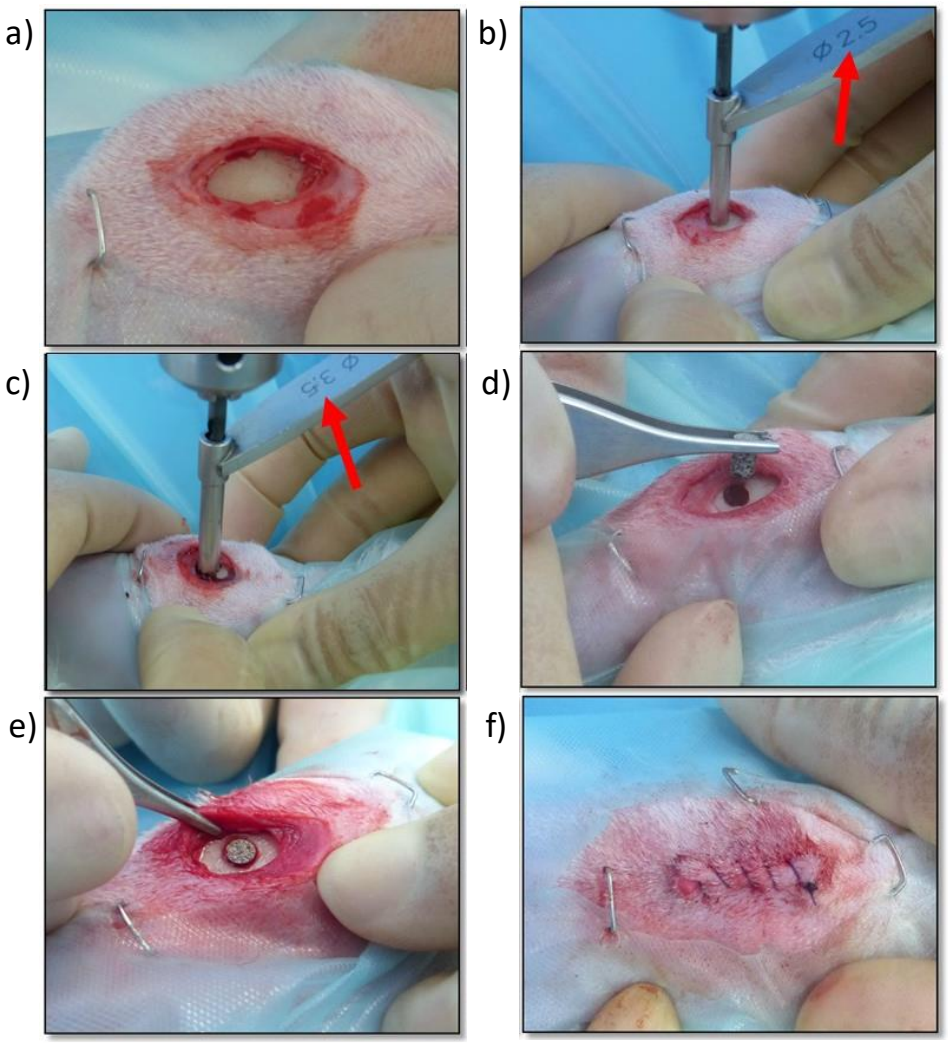

Figure 8. Screen photographic sequence of the surgical method: a) Medial approach to the proximal aspect of the right tibia b) Creating a monocortical bone defect with a 2.5mm drill bit., c) Enlarging the monocortical bone defect with a 3.5mm drill bit., d) Placing the titanium implant in the monocortical bone defect., e) Checking the adequate placement and fixation of the titanium implant, f) Surgical wound sutured with a continuous pattern.

For the surgical implantation (Figure 8), with the animals in dorsal recumbency, both tibial regions were clipped and subsequently scrubbed with chlorhexidine gluconate solution 4% for an aseptic preparation of the surgical field. Afterwards, the medial aspect of the proximal tibia was exposed through a limited skin and subcutaneous incision. Using drill bits of increasing size and under copious irrigation with physiological saline a final monocortical bone defect of 3.mm in diameter was generated on a craneocaudal midpoint in the medial aspect of the proximal tibia. Cylindrical porous titanium implants were placed inside these defects by "press-fit" mode until flushed with the cortical surface. The subcutaneous tissue and the skin were sutured in layers by using a standard suture pattern with synthetic resorbable sutures (Vycril 3/0, Ethicon, Johnson & Johnson, USA). Immediately after surgery and with the animals still under general anesthesia tibial mediolateral and craniocaudal radiographs were taken to confirm the correct location of the implants.

4.5. Euthanasia

The animals were euthanized at the scheduled survival times with an overdose of sodium pentobarbitone (200mg/kg/i.v.) according to the legislation of the American Veterinary Medical Association. (AVMA). A pre-euthanasia sedation of midazolam (0.50 mg/kg s.c.) and medetomidine (0.05 mg/kg s.c) was used for animal welfare reasons.

Then, tibiae bones were completely harvested and the peripheral soft tissue was removed. Finally, craniocaudal and medio lateral radiographs of the bone samples were performed.

4.6. Samples preparation

Bone tibiae samples were individually identified and stored by immersion in neutral buffered 10% formalin solution for 3 weeks in order to assure proper bone fixation and tissue preservation. After fixation time, samples were rinsed in running tap water during 15 min to eliminate any fixative agent residues. After rinsing, samples underwent a progressive dehydration process by immersion in increasing concentrations of ethanol in aqueous solutions (from 30% to 100% v/v) with constant stirring at 50 rpm. Once dehydrated, samples were immersed in ethanol solutions with increasing concentrations of methyl-methacrylate resin Technovit 7200 (Kulzer-Heraeus, Hanau, Germany) (from 30% to 100%) with constant stirring at 50 rpm. Finally, samples were kept under vacuum conditions for 24 hours to ensure resin penetration into the tissues and subsequently embedded in a 100% resin solution by photo-polymerization using a light control unit Histolux (Kulzer-Heraeus, Hanau, Germany), following a 24h process of visible and UV light exposure.

A total of 36 samples were obtained and were cut in 2 halves to expose the metallic scaffold: 15 implants were cut perpendicularly to the longitudinal axis of the scaffold (transversal mode), and 3 implants were cut following its longitudinal axis (longitudinal mode). Exposed metallic surfaces were polished with SiC abrasive papers (800, 1200, 4000 index mesh) using a Exakt-400 CS grinding machine (Exakt, Norderstedt, Germany) to obtain smooth and scratch-less surfaces for SEM observation. For each postoperative period–group, a total of 15 implants were used to obtain samples in scaffold cross-section mode, and 3 samples to obtain samples cut in scaffold longitudinal axis.

4.7. Obtaining images of the samples by SEM.

The polished samples were carbon-coated by sputtering and then observed by scanning electron microscopy (SEM) suing a Neon40 Crossbeam™ FIB-SEM (Carl Zeiss, Dresden, Germany) with backscattered-electron (BSE) detector. Observation conditions were 15 kV of potential with a working distance of about 8 mm to achieve a resolution up to 1.1 nm in SEM-BSE mode.

The SEM observation was performed by carrying out a sequential scan of the surface acquiring high magnification pictures and then merged using SMART STITCH Software (Carl Zeiss, Dresden, Germany) and mage-J 1.46 Software (NIH, Fredrick, MD, USA). The obtained images were individually processed using Image-J and (Adobe Systems, Ireland) in order to ensure correct histomorphometry evaluation.

4.8. SEM quantitative evaluation method.

Stitched images obtained by SEM were calibrated and analyzed by using Image J software. All images were identically acquired (see SEM/FIB settings) and post-processed. Every image was thresholded to separate metallic implant area, void porous space, and newly formed bone tissue inside the initial defect created in surgery procedure. Thus,

752 thresholded binary images derived from the grey-scaled original image were created for
753 each sample.
754 Image J was used to quantify the area (percentage) occupied by every thresholded
755 tissue and/or material present in each sample from binary data: metallic implant area
756 (white), void porous space inside the defect (black) and the newly formed bone tissue
757 (grey scale) present in the free space available for bone growth, as can be seen in Figure 9.
758 The latter was crucial to evaluate the amount of bony tissue generated in the internal and
759 interconnected porosity, so the more porosity the more space available for the bone to
760 grow.
761 Outermost newly formed bone tissue can be differentiated from pre-existing host
762 bone tissue due to differences in gray scale values, microarchitecture (growth bands dis-
763 play) and microstructure (maturity and porosity) of the tissues. The threshold applied to
764 every tissue/area in every image was individually selected for each sample and performed
765 by the same user. All samples were previously coded to ensure blind analysis.
766
767

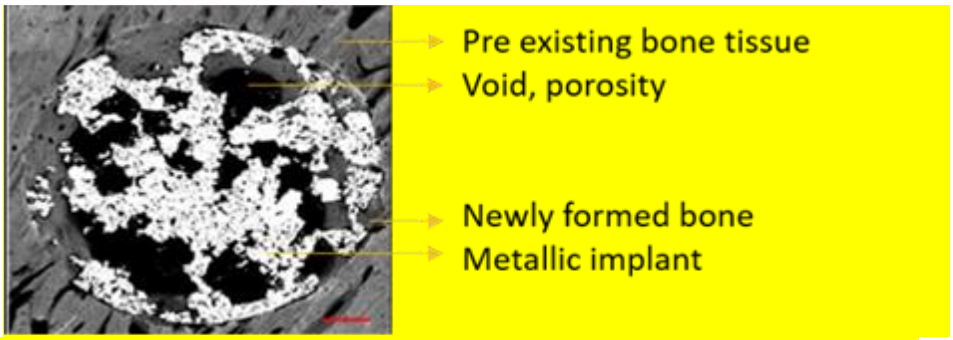

768
769 **Figure 9.** Stitched gray scale image obtained by SEM analysis detailing the different materials identified.

770 The bone in growth was characterized by the newly formed bone and was quantified
771 in 3 different regions of interest (ROI) inside the implants: outer ROI (ROI-1), middle ROI
772 (ROI-2) and center ROI (ROI-3); where each ROI radius was a third part of the implant
773 radius (**¡Error! No se encuentra el origen de la referencia.**). ROIs analysis were performed
774 taking into account the available space existent within the interconnected porosity to ful-
775 fill with newly formed bone. All newly formed bone inside the whole implant was quan-
776 tified and named as "Total Ingrowth".
777 The Bone on-growth assessment was performed by "outer" bone and BIC (Bone im-
778 plant contact) parameters. The outer bone was identified as the newly bone formed
779 around the implant: from the external implant perimeter up to 100 μm radially towards
780 outside. The bone tissue loss, due to thermal necrosis caused by surgical milling and by
781 the vascular ischemia produced during the implantation, was taken into account. BIC was
782 evaluated as direct contact between mineralized newly formed bone and the external im-
783 plant surface. A scheme is shown in Figure 10.
784 All samples were analyzed with the same methodology. ROIs were automatically
785 drawn to be equivalent in whole samples. All samples were evaluated by 3 different in-
786 dependent researchers, first in real size and then in detail at different magnifications.
787

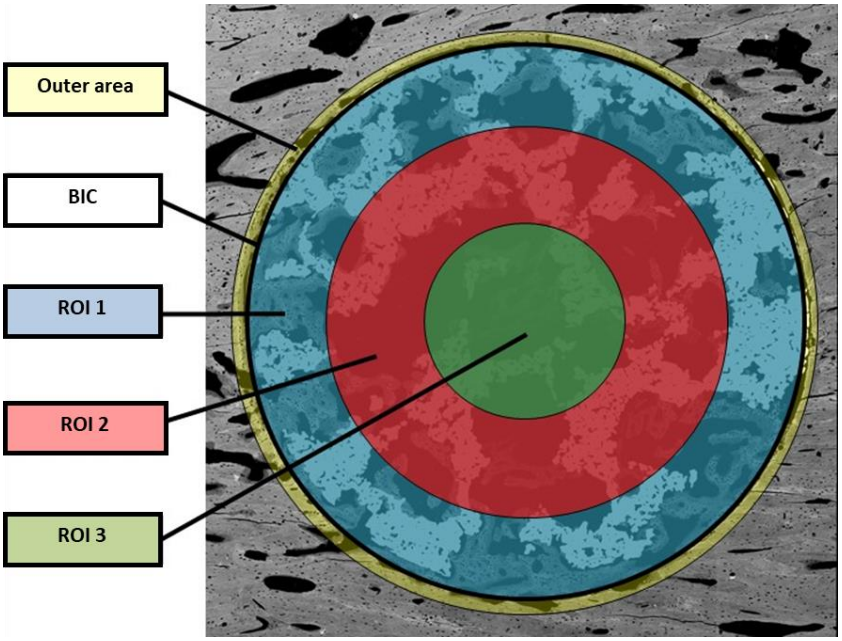

Figure 10. Graphical Scheme for assessment of BIC and ROI values.

4.9. Qualitative evaluation for transversal images

The following parameters were analyzed:

- Quality and maturity of external newly formed bone.
- Quality and maturity of external newly formed bone in direct contact with external implant surface (BIC).
- Quality and maturity of external newly formed bone inside the interconnected scaffold porosity.
- Penetration of newly formed bone inside the scaffold.
- Newly formed bone contact within the metallic scaffold surface.
- Bone filling inside the scaffold micro cavities and micro pores.
- Assessment of the bone progress towards the scaffold center.
- Presence of necrotic or soft tissue.

4.10. Qualitative evaluation for longitudinal images

Three samples of each-postoperative period-group (4 and 12 weeks) were used to obtain longitudinal images and perform a qualitative analysis. The newly formed bone tissue and its origin (periosteum, cortical and/or endosteum) were analyzed in the three experimental groups samples (TCG, PAG, CG).

4.11. Statistical analysis

Histomorphometrical results are set out as mean ± standard error of the mean. All numerical values followed a normal distribution as Anderson-Darling and Kolmogorov-Smirnov tests showed.

Statistical analysis was performed by one-way ANOVA followed by Tukey post hoc tests using the GraphPad Prism software (ANOVA, La Jolla, CA, USA). Statistically significant differences were considered for $p < 0,05$.

5. Conclusions

Albeit after both 4 and 12 weeks of implantation, no statistically significant differences were observed between the untreated scaffolds and the bioactivation treatments, quantitative analysis revealed higher values for the biotreated surfaces when comparing ROIs, especially the outer one, as well as the inner volume filling or the scaffolds.

However, when quantitatively comparing the two bioactivation methods, the PEPTIDE treatment strategy seems to be the best option to enhance and accelerate bone tissue growth over the implant surface according to the BIC values achieved, while the THERMO-CHEMICAL strategy yielded better filling values in the inner core areas of the scaffolds. These results suggest that both strategies contribute to enhance porous metallic implants stability and osteointegration, and combination of both strategies might be worth pursuing.

From a qualitative point of view, the bioactivation of titanium implants through the innovative peptide treatment used in this study generated an osseoregenerative response constituted by a greater amount of a more mature newly formed bone tissue when compared to the response obtained by the thermal-chemical and control groups. However, this greater and rapidly maturing new bone formation is not accompanied by a greater adhesion to the titanium pores within the inner core of the implant.

Concerning to the implantation time, the presence of woven bone tissue was observed after 4 weeks of implantation, together with lamellar bone tissue in some areas of the samples from the control group both within micro and macropores. After 12 weeks, the results showed more mature newly formed bone tissue growing towards the inner areas of the scaffolds, with predominant presence of lamellar bone tissue.

Furthermore, the whole innovative experimental design, including both the protocol for the surgical insertion of implants in bone and the protocol for digital histo-morphometrical assessment and tridimensional evaluation of the scaffolds proved to be both efficient and effective. The sequence of quantitative results allows a comprehensive analysis of the advancement of the osseointegration process and sustains the ulterior qualitative observation of the maturity and ultrastructural patterns of bone regeneration. This way, the reported protocol for the assessment of the evolution of osseoconduction and osseointegration of the implants can be considered as an evaluation standard in subsequent studies with similar objectives.

Author Contributions: For research articles with several authors, a short paragraph specifying their individual contributions must be provided. The following statements should be used "Conceptualization, JF, JG, ER, JC and JGM.; methodology, MCM, MO, MP; software, AB, JC, CMM, JG; validation, CC, JF,MP, MM and KR; formal analysis, MCM, JF,JG.; investigation, KR, MO, MM, MP, MCM.; resources, JG, JC, ER; data curation, JG.; writing—original draft preparation, KR, JF; writing—review and editing, CMM, MCM, MP, JG.; visualization, AB; supervision, MP, JG.; project administration, JC; funding acquisition, JC, JG All authors have read and agreed to the published version of the manuscript."

Ethical approval: This article does not contain any studies with human participants. The in vivo studies was approved for this study by the Faculty of Veterinary Sciences of the Universitat Autonoma de Barcelona (Spain) with reference PUAB1/7234.

Informed consent: For this type of study, formal consent is not required.

Conflicts of Interest: The authors reject any conflicts of interest.

Acknowledgments: The authors thank the Spanish Government for financial support through a Ramon y Cajal grant of C.M.-M. (RYC-2015-18566) and Projects No. RTI2018-098075-B-C21, RTI2018-098075-BC22 and PID2020-114019RB-I00/AEI/10.13039/501100011033, cofounded by the

EU through the European Regional Development Funds (MINECO-FEDER, EU). Authors also acknowledge Generalitat de Catalunya for funding through the 2017SGR-1165 and 2017SGR708 projects.

References

1. Ahmadi SM, Hedayati R, Li Y, Lietaert K. Fatigue performance of additively manufactured meta-biomaterials: the effects of topology and material type. Acta Biomater., 2018, 65: 292-304. ISSN 1742-7061, https://doi.org/10.1016/j.actbio.2017.11.014.
2. Bobbert FSL, Lietaert K, Eftekhari AA, Pouran B. Additively manufactured metallic porous biomaterials based on minimal surfaces: A unique combination of topological, mechanical, and mass transport properties. Acta Biomater., 2017, 53: 572-584. ISSN 1742-7061, https://doi.org/10.1016/j.actbio.2017.02.024.
3. Bidan CM, Kommareddy KP, Rumpler M, Kollmannsberger P, Bréchet YJM, Fratzl P. How Linear Tension Converts to Curvature: Geometric Control of Bone Tissue Growth. PLoS ONE 2012, 7(5): e36336. https://doi.org/10.1371/journal.pone.0036336.
4. Bidan CM, Kommareddy KP, Rumpler M, Kollmannsberger P, Fratzl P, Dunlop JW. Geometry as a factor for tissue growth: towards shape optimization of tissue engineering scaffolds. Adv Healthc Mater. 2013, 2(1):186-94. doi: 10.1002/adhm.201200159.
5. Zadpoor AA, Bone tissue regeneration: the role of scaffold geometry, Biomaterials Science, 2015, 3 (2): 231-245.
6. Fernandez-Yague MA, Abbah SA, McNamara L, Zeugolis DI, Pandit A, Biggs MJ. Biomimetic approaches in bone tissue engineering: Integrating biological and physicomechanical strategies. Advanced Drug Delivery Reviews, 2015, 84: 1-29. https://doi.org/10.1016/j.addr.2014.09.005.
7. Dias M, Fernandes P, Guedes J, Hollister S, Permeability analysis of scaffolds for bone tissue engineering, Journal of biomechanics, 2012; 45 (6): 938-944. https://doi.org/10.1016/j.jbiomech.2012.01.019.
8. Hollister SJ, Porous scaffold design for tissue engineering, Nature materials, 2005, 4 (7): 518-524. https://doi.org/10.1038/nmat1421.
9. Karande, T.S., Ong, J.L., Agrawal, C.M. Diffusion in Musculoskeletal Tissue Engineering Scaffolds: Design Issues Related to Porosity, Permeability, Architecture, and Nutrient Mixing. Ann Biomed Eng 2004, 32, 1728–1743. https://doi.org/10.1007/s10439-004-7825-2.
10. Ripamonti U. Osteoinduction in porous hydroxyapatite implanted in heterotopic sites of different animal models. Biomaterials, 1996, 17 (1): 31-35. https://doi.org/10.1016/0142-9612(96)80752-6.
11. Zhao X, Courtney JM, Qian H. Bioactive Materials in Medicine: Design and applications. First edition. Sawston, Cambrigde. Woodhead Publishing; 2011.
12. Ambard AJ, Mueninghoff L. Calcium phosphate cement: review of mechanical and biological properties. J Prosthodont., 2006, 15 (5): 321-328. https://doi.org/10.1111/j.1532-849X.2006.00129.x.
13. Khodaei M, Fathi M, Meratian M et al. The effect of porosity on the mechanical properties of porous titanium scaffolds: Comparative study on experimental and analytical values. Materials Research Express, 2018, 5(5). https://doi.org/10.1088/2053-1591/aabfa2.
14. Taniguchi N, Fujibayashi S, Takemoto. Effect of pore size on bone ingrowth into porous titanium implants fabricated by additive manufacturing: An in vivo experiment. Materials Science and Engineering: C, 2016 59: 690-701. https://doi.org/10.1016/j.msec.2015.10.069.
15. Van Hooreweder B, Apers Y, Lietaert K, Kruth JP. Improving the fatigue performance of porous metallic biomaterials produced by Selective Laser Melting, Acta Biomaterialia, 2017, 47: 193-202, ISSN 1742-7061, https://doi.org/10.1016/j.actbio.2016.10.005.
16. Caparrós C, Guillem-Martí J, Molmeneu M, Punset M, Calero JA, Gil FJ. Mechanical properties and in vitro biological response to porous titanium alloys prepared for use in intervertebral implants. Journal of the Mechanical Behavior of Biomedical Materials, 2014, 39:. 79-86. ISSN 1751-6161, https://doi.org/10.1016/j.jmbbm.2014.05.029.
17. Li, G., Wang, L., Pan, W. In vitro and in vivo study of additive manufactured porous Ti6Al4V scaffolds for repairing bone defects. Sci Rep 2016, 6: 34072. https://doi.org/10.1038/srep34072.
18. Stock JV der, Full regeneration of segmental bone defects using porous titanium implants loaded with BMP-2 containing fibrin gels. Eur. Cell. Mater., 2015, 29: 141-154. ISSN 1473-2262.
19. Hasart O, Perka C, Lehnigk R, Tohtz S. Rekonstruktion größerer Pfannendefekte mit metallischen Augmentaten – Trabecular Metal Technology. Operative Orthopädie Und Traumatologie, 2010, 22(3): 268–277. https://doi.org/10.1007/s00064-010-8026-9.

20. Pałka, K. and Pokrowiecki, R. Porous Titanium Implants: A Review. Adv. Eng. Mater., 2018, 20: 1700648. https://doi.org/10.1002/adem.201700648.
21. Riew K.D, Rhee J.M. The use of titanium mesh cages in the cervical spine. Clinical Orthopaedics and Related Research, 2002, 394: 47-54.
22. Dabrowski B, Swieszkowski W, Godlinski D, Kurzydlowski J. Highly porous titanium scaffolds for orthopaedic applications. Journal of Biomedical Materials Research Part B: Applied Biomaterials, 2010, 95B (1): 53–61. https://doi.org/10.1002/jbm.b.31682.
23. Karageorgiou, V.; Kaplan, D. Porosity of 3D biomaterial scaffolds and osteogenesis. Biomaterials 2005, 26, 5474–5491. https://doi.org/10.1016/j.biomaterials.2005.02.002,
24. Khosla, S., Westendorf, J.J., and Modder, U.I. Concise review: Insights from normal bone remodeling and stem cell-based therapies for bone repair. Stem Cells, 2010, 28 : 2124. https://doi.org/10.1002/stem.546.
25. Ng J, Spiller K, Bernhard J and Vunjak-Novakovic G. Biomimetic Approaches for Bone Tissue Engineering. Tissue Eng Part B Rev., 2017, 23 (5): 480-493. https://doi.org/10.1089/ten.teb.2016.0289.
26. M. Ortiz-Hernandez, K. S. Rappe, M. Molmeneu, C. Mas-Moruno, J. Guillem-Marti, M. Punset, C. Caparros, J.A. Calero, J. Franch, M. Fernandez-Fairen and J. Gil. Two Different Strategies to Enhance Osseointegration in Porous Titanium: Inorganic Thermo-Chemical Treatment Versus Organic Coating by Peptide Adsorption. Int. J. Mol. Sci. 2018, 19 (9): 2574. https://doi.org/10.3390/ijms19092574.
27. L. Jian-guo, Z. Yun-fei and. Mo. Preparation of porous Ti35Nb alloy and its mechanical properties under monotonic and cycling loading. Trans. Nonferrous Met. Soc. China, 2010, 20: 390-394. https://doi.org/10.1016/S1003-6326(09)60151-5.
28. B.D. Ratner, A.S. Hoffman, F.J. Schoen, J.E. Lemons et al, Biomaterials Science: An introduction to materials in medicine, Third ed., Academic press, UK, 2013.
29. Krishna, B.V.; Bose, S.; Bandyopadhyay, A. Low stiffness porous Ti structures for load-bearing implants. Acta Biomater. 2007, 3: 997–1006. https://doi.org/10.1016/j.actbio.2007.03.008.
30. Park J.Y., Park S.H., Kim M.G., Park SH., Yoo T.H., Kim M.S. Biomimetic Scaffolds for Bone Tissue Engineering. In: Noh I. (eds) Biomimetic Medical Materials. Advances in Experimental Medicine and Biology, 2018, 1064. Springer, Singapore. https://doi.org/10.1007/978-981-13-0445-3_7.
31. S. Bernard, V. K. Balla, S. Bose and A. Bandyopadhyay. Compression fatigue behavior of laser processed porous NiTi alloy. J. Mech. Behav. Biomed. Mater., 2012, 13: 62-68. ISSN 1751-6161, https://doi.org/10.1016/j.jmbbm.2012.04.010.
32. X.P. Tan, Y.J. Tan, C.S.L. Chow, S.B. Tor and W.Y. Yeong. Metallic powder-bed based 3D printing of cellular scaffolds for orthopaedic implants: A state-of-the-art review on manufacturing topological design, mechanical properties and biocompatibility. Mater. Sci. Eng. C., 2017, 76: 1328-1343. https://doi.org/10.1016/j.msec.2017.02.094.
33. Y. Hirata, Y. kaInaba, N. Kobayashi, H. Ike. Fujimaki, T. Saito. Comparison of Mechanical Stress and Change in Bone Mineral Density Between Two Types of Femoral Implant Using Finite Element Analysis. The Journal of Arthroplasty, 2013, 28: 1731-1735. https://doi.org/10.1016/j.arth.2013.04.034.
34. L. Shi, L. Shi, L. Wang, Y. Duan, et al. The Improved Biological Performance of a Novel Low Elastic Modulus Implant. PLoS One. 2013; 8(2): e55015. https://doi.org/10.1371/journal.pone.0055015.
35. J. Duyck, K. Vandamme, L.Geris, H.Van Oosterwyck, et al. The influence of micro-motion on the tissue differentiation around immediately loaded cylindrical turned titanium implants. Archives of Oral Biology, 2006, 51: 1-9. https://doi.org/10.1016/j.archoralbio.2005.04.003.
36. Wang D, Li Q, Xu M. A novel approach to fabrication of three-dimensional porous titanium with controllable structure. Materials Science and Engineering: C, 2017, 71: 1046-1051.
37. Oh, I.H.; Nomura, N.; Masahashi, N.; Hanada, S. Mechanical properties of porous titanium compacts prepared by powder sintering. Scripta Mater. 2003, 49: 1197–1202. ISSN 1359-6462, https://doi.org/10.1016/j.scriptamat.2003.08.018.
38. Li, J.P.; Li, S.H.; van Blitterswijk, C.A.; de Groot, K. A novel porous Ti6Al4V: Characterization and cell attachment. J. Biomed. Mater. Res., 2005, 73: 223–233. https://doi.org/10.1002/jbm.a.30278.
39. Zhang, X.; Ayers, R.A.; Thorne, K.; Moore, J.J.; Schowengerdt, F. Combustion synthesis of porous materials for bone replacement. Biomed. Sci. Instrum. 2001, 37: 463–468.
40. Ryan, G.E.; Pandit, A.S.; Apatsidis, D.P. Porous titanium scaffolds fabricated using a rapid prototyping and powder metallurgy technique. Biomaterials 2008, 29: 3625–3635. https://doi.org/10.1016/j.biomaterials.2008.05.032.
41. Dewidar, M.M.; Lim, J.K. Properties of solid core and porous surface Ti-6Al-4V implants manufactured by powder metallurgy. J. Alloys Compd. 2008, 454: 442–446. https://doi.org/10.1016/j.jallcom.2006.12.143.
42. Vasconcellos, L.M.; Oliveira,M.V.; Alencastro Graça,M.L.; Vaconcellos, L.G.; Carvalho, Y.R.; Cairo, C.A. Porous titanium scaffolds produced by powder metallurgy for biomedical applications. Mater. Res. 2008, 11: 275–280.
43. Wu, S.; Liu, X.; Yeung, K.W.; Liu, C.; Yang, X. Biomimetic porous scaffolds for bone tissue engineering.Mater. Sci. Eng. R 2014, 80: 1–36.

44. Li, J.P.; deWijn, J.R.; van Blitterswijk, C.A.; de Groot, K. Porous Ti6Al4V scaffold directly fabricating by rapid prototyping: Preparation and in vitro experiment. Biomaterials 2006, 27: 1223–1235. https://doi.org/10.1016/j.biomaterials.2005.08.033.
45. Heinl, P.; Müller, L.; Körner, C.; Singer, R.F.; Müller, F.A. Cellular Ti-6Al-4V structures with interconnected macro porosity for bone implants fabricated by selective electron beam melting. Acta Biomater. 2008, 4: 1536–1544. https://doi.org/10.1016/j.actbio.2008.03.013.
46. Ponader, S.; von Wilmowsky, C.; Widenmayer, M.; Lutz, R.; Heinl, P.; Körner, C.; Singer, R.F.; Nkenke, E.; Neukam, F.W.; Schlegel, K.A. In vivo performance of selective electron beam-melted Ti-6Al-4V structures. J. Biomed. Mater. Res. A 2010, 92: 56–62. https://doi.org/10.1002/jbm.a.32337.
47. X.Y. Cheng, S.J. Li, L.E. Murr, Z.B. Zhang, Y.L. Hao, R. Yang, F. Medina, R.B. Wicker, Compression deformation behavior of Ti–6Al–4V alloy with cellular structures fabricated by electron beam melting, Journal of the Mechanical Behavior of Biomedical Materials, 2012, 16: 153-162, ISSN 1751-6161, https://doi.org/10.1016/j.jmbbm.2012.10.005.
48. S.J. Li, L.E. Murr, X.Y. Cheng, Z.B. Zhang, Y.L. Hao, R. Yang, F. Medina, R.B. Wicker, Compression fatigue behavior of Ti–6Al–4V mesh arrays fabricated by electron beam melting, Acta Materialia, 2012, 60: 793-802, ISSN 1359-6454, https://doi.org/10.1016/j.actamat.2011.10.051.
49. N.W. Hrabe, P. Heinl, B. Flinn, C. Körner, et al. Compression-compression fatigue of selective electron beam melted cellular titanium (Ti-6Al-4V). J. Biomed. Mater. Res. Part B, 2012, 99: 313-320. https://doi.org/10.1002/jbm.b.31901.
50. S. Zhao, S.J. Li, W.T. Hou, Y. L. Hao, et al. The influence of cell morphology on the compressive fatigue behavior of Ti-6Al-4V meshes fabricated by electron beam melting. J. Mech. Behav. Biomed. Mater., 2016, 59: 251-264.
51. Mullen, L.; Stamp, R.C.; Brooks,W.K.; Jones, E.; Sutcliffe, C.J. Selective laser melting: A regular unit cell approach for the manufacture of porous, titanium, bone ingrowth constructs, suitable for orthopedic applications. J. Biomed. Mater. Res. B Appl. Biomater. 2009, 89: 325–334. Int. J. Mol. Sci. 2018, 19: 2574 15 of 17. https://doi.org/10.1002/jbm.b.31219.
52. Santos, E.; Osakada, K.; Shiomi, M.; Kitamura, Y.; Abe, F. Microstructure and mechanical properties of pure titanium models fabricated by selective laser melting. Proc. Inst. Mech. Eng. Part C 2004, 218: 711–719. https://doi.org/10.1243/0954406041319545.
53. F. Brenne, T. Niendorf and H. Maier. Additively manufactured cellular structures: Impact of microstructure and local strains on the monotonic and cyclic behavior under uniaxial and bending load. J. Mater. Process. Tech., 2013, 213 (9): 1558-1564. ISSN 0924-0136, https://doi.org/10.1016/j.jmatprotec.2013.03.013.
54. B. Gorny, T. Niendorf, J. Lackmann, M. Thoene, T. Troester, H.J. Maier, In situ characterization of the deformation and failure behavior of non-stochastic porous structures processed by selective laser melting, Materials Science and Engineering: A, 2011, 528 (27): 7962-7967, ISSN 0921-5093, https://doi.org/10.1016/j.msea.2011.07.026.
55. C. Yan. Evaluations of cellular lattice structures manufactured using selective laser melting. International Journal ao Machine Tools and Manufacture, 2012, 62: 32-38.
56. R. Wauthle, J.P. Kruth, J. Schrooten and M. Mulier. Industrialization of selective laser melting for the production of porous titanium and tantalum implants, 120 pp, PhD, KU Leuven, 2014.
57. Shishkovsky, I.V.; Volova, L.T.; Kuznetsov, M.V.;Morozov, Y.G.; Parkin, I.P. Porous biocompatible implants and tissue scaffolds synthesized by selective laser sintering from Ti and NiTi. J. Mater. Chem. 2008, 18: 1309–1317. https://doi.org/10.1039/B715313A.
58. Wen, C.E.; Yamada, Y.; Shimojima, K.; Chino, Y.; Asahina, T. Mabuchi,M. Processing andmechanical properties of autogenous titaniumimplantmaterials. J.Mater. Sci. Mater. Med. 2002, 13: 397–401.
59. Bram, M.; Stiller, C.; Buchkremer, P.H.; Stöver, D.; Baur, H. High-porosity titanium, stainless steel, and superalloy parts. Adv. Eng. Mater. 2000, 2: 196–199. https://doi.org/10.1002/(SICI)1527-2648(200004)2:4<196::AID-ADEM196>3.0.CO;2-K.
60. Ryan, G.; Pandit, A.; Apatsidis, D.P. Fabrication methods of porous metal for use in orthopedic applications. Biomaterials 2006, 27: 2651–2670. https://doi.org/10.1016/j.biomaterials.2005.12.002.
61. Caparrós, C.; Ortiz-Hernandez, M.; Molmeneu, M.; Punset, M.; Calero, J.A.; Aparicio, C.; Fernández-Fairén, M.; Perez, R.; Gil, F.J. Bioactive macroporous titanium implants highly interconected. J. Mater. Sci. Mater. Med. 2016, 27: 151. https://doi.org/10.1007/s10856-016-5764-8.
62. Alvarez, K.; Nakajima, H. Metallic Scaffolds for Bone Regeneration. Materials 2009, 2: 790-832. https://doi.org/10.3390/ma2030790.
63. Rao, P.J.;Walsh,W.R.; Pellitier,M.H.;Mobbs, R.J. Spine interbody implants: Material selection andmodification, functionalization and bioactivation of surfaces to improve osseointegration. Orthop. Surg. 2014, 6: 81–89. https://doi.org/10.1111/os.12098.
64. Williams, D.F. There is no such thing as a biocompatible material. Biomaterials 2014, 35: 10009–10014.
65. L. Giner, M. Mercade, S. Torrent, M. Punset, R. Pérez-Antoñanzas, L. Delgado, F.J. Gil. Double acid etching treatment of dental implants for enhanced biological properties. J Appl Biomater Funct Mater. 2018, 16 (2): 83-89. doi: 10.5301/jabfm.5000376.

66. Zhao, C., Zhu, X., Liang, K., Ding, J., Xiang, Z., Fan, H., & Zhang, X. Osteoinduction of porous titanium: A comparative study between acid-alkali and chemical-thermal treatments. Journal of Biomedical Materials Research Part B: Applied Biomaterials, 2010, 95B(2): 387–396. doi:10.1002/jbm.b.31728.
67. Lopez-Heredia, M.A.; Sohier, J.; Gaillard, C.; Quillard, S. Rapid prototyping porous titanium coated with calcium phosphate as a scaffold for bone tissue engineering. Biomaterials 2008, 29: 2608–2615. https://doi.org/10.1016/j.biomaterials.2008.02.021.
68. Tamaddon, M.; Samizadeh, S.; Wang, L.; Blunn, G.; Liu, C. Intrinsic osteoinductivity of porous titanium scaffold for bone tissue engineering. Int. J. Biomater. 2017. 5093063. https://doi.org/10.1155/2017/5093063.
69. Thalgott, J.S.; Giuffre, J.M.; Klezl, Z.; Timlin, M. Anterior lumbar interbody fusion with titanium mesh cages, coralline hydroxyapatite, and demineralized bone matrix as part of a circumferential fusion. Spine J. 2002, 2: 63–69.
70. J. Guillem-Marti, N. Cinca, M. Punset, I. García Cano, F.J. Gil, J.M. Guilemany, S Dost. Porous titanium-hydroxyapatite composite coating obtained on titanium by cold gas spray with high bond strength for biomedical applications. Colloids and Surfaces B: Biointerfaces, 2019, 180: 245–253. https://doi.org/10.1016/j.colsurfb.2019.04.048.
71. Jung Kim K., Iwase M., Kotake S., Itoh T. Effect of bone marrow grafting on the titanium porous-coated implant in bilateral total knee arthroplasty, Acta Orthopaedica, 2007, 78 (1): 116-122, DOI: 10.1080/17453670610013510
72. Kroese-Deutman, H.C.; Vehof, J.W.; Spauwen, P.H.; Stoelinga, P.J.; Jansen, J.A. Orthotopic bone formation in titanium fiber mesh loaded with platelet-rich plasma and placed in segmental defects. Int. J. Oral Maxillofac. Surg. 2008, 37: 542–549. https://doi.org/10.1016/j.ijom.2008.01.009.
73. Jansen, J.A.; Vehof, J.W.; Ruhé, P.Q.; Kroeze-Deutman, H.; Kuboki, Y.; Takita, H.; Hedberg, E.L.; Mikos, A.G. Growth factor-loaded scaffolds for bone engineering. J. Controll. 2005, 101: 127–136. https://doi.org/10.1016/j.jconrel.2004.07.005.
74. Matsuzaka, K.; Yoshinari, M.; Kokubu, E.; Shimono, M.; Yamada, Y.; Mabuchi, M.; Inoue, T. Bone formation in titanium porous scaffold with immobilization of BMP-2. J. Oral Tissue Eng. 2005, 2: 60–65. https://doi.org/10.11223/jarde.2.60.
75. De Peppo, G.M.; Palmquist, A.; Borchardt, P.; Lennerås, M.; Hyllner, J.; Snis, A.; Lausmaa, J.; Thomsen, P.; Karlsson, C. Free-form-fabricated commercially pure Ti and Ti6Al4V porous scaffolds support the growth of human embryonic stem cell-derived mesodermal progenitors. Sci. World J. 2012, 646417. https://doi.org/10.1100/2012/646417.
76. Zhang, W.; Walboomers, X.F.; van Kuppevelt, T.H.; Daamen, W.F.; Bian, Z.; Jansen, J.A. The performance of human dental pulp stemcells on different three dimensional scaffolds materials. Biomaterials 2006, 27: 5658–5668.
77. Mas-Moruno, C.; Fraioli, R.; Rechenmacher, F.; Neubauer, S.; Kapp, T.G.; Kessler, H. $\alpha v\beta 3$- or $\alpha 5\beta 1$-integrin-selective peptidomimetics for surface coating. Angew. Chem. Int. Ed. 2016, 55: 7048–7067. https://doi.org/10.1002/anie.201509782.
78. Mas-Moruno, C. Surface functionalization of biomaterials for bone tissue regeneration and repair. In Peptides and Proteins as Biomaterials for Tissue Regeneration and Repair;Martins, C., Barbosa,M., Eds.; Elsevier: Oxford, UK, 2018: 73–100. https://doi.org/10.1016/B978-0-08-100803-4.00003-6.
79. Karakoy, M.; Guttepe, E.; Pansdey, S.; Kharhab, M.; Gracias, D. Silane Surface modification for improved bioadhesion of esophageal stents. Appl. Surf. Sci. 2014, 311: 684–689. https://doi.org/10.1016/j.apsusc.2014.05.136.
80. Vo Dinh, T. (Ed.) Nanotechnology in Biology and Medicine. Methoods, Devices and Applications; CRC Press Book: Natwick, MA, USA, 2010; ISBN 9781439893784.
81. Yoon, S.T.; Konopka, J.A.; Wang, J.C.; Youssef, J.A.; Meisel, H.J.; Brodke, D.S.; Park, J.B. ACDF graft selection by surgeons: Survey of AOSpine members. Glob. Spine J. 2017, 7: 410–416. Int. J. Mol. Sci. 2018, 19, 2574 16 of 17.
82. Auermheimer J, Zukowski D, Dahmen C, Kantlehner, M. Titanium implant materials with improved biocompatibility through coating with phosphonate-anchored cyclic RGD peptides. Chem BioChem, 2005, 6 (11): 2034–2040. https://doi.org/10.1002/cbic.200500031.
83. Cirera A, Sevilla P, Manzanares MC, Franch J, Galindo-Moreno P, Gil J. Osseointegration around dental implants biofunctionalized with TGFβ-1 inhibitor peptides: an in vivo study in beagle dogs. J Mater Sci Mater Med. 2020, 31(8): 62. doi: 10.1007/s10856-020-06397-3
84. Ivanoff, C.J.;Widmark, G.; Hallgren, C.; Sennerby, L.;Wennerberg, A. Histologic evaluation of the bone integration of TiO2 blasted and turned titaniummicroimplants in humans. Clin. Oral Implants Res. 2001, 12: 128–134. https://doi.org/10.1034/j.1600-0501.2001.012002128.x
85. Kokubo, T.; Yamaguchi, S. Novel bioactive titanate layers formed on Timetal and its alloys by chemical treatments. Materials. 2010, 3: 48–63. https://doi.org/10.3390/ma3010048.
86. Takadama, C.H.; Kim, H.M.; Kokubo, T.; Nakamura, T. TEM-EDX study of mechanism of bonelike apatite formation on bioactive titanium metal in simulated body fluid. J. Biomed. Mater. Res. 2001, 57: 441–448. https://doi.org/10.1002/1097-4636(20011205)57:3<441::AID-JBM1187>3.0.CO;2-B.
87. Mas-Moruno, C.; Dorfner, P.M.; Manzenrieder, F.; Neubauer, S.; Reuning, U.; Burgkart, R.; Kessler, H. Behavior of primary human osteoblasts on trimmed and sandblasted Ti6Al4V surfaces functionalized with integrin _v_3-selective cyclic RGD peptides. J. Biomed. Mater. Res. A 2013, 101: 87–97. https://doi.org/10.1002/jbm.a.34303.
88. Mas-Moruno, C.; Fraioli, R.; Albericio, F.; Manero, J.M.; Gil, F.J. Novel peptide-based platform for the dual presentation of biologically active peptidemotifs on biomaterials. ACS Appl. Mater. Interfaces 2014, 6: 6525–6536. DOI: 10.1021/am5001213.

89. Mas-Moruno, C.; Garrido, B.; Rodriguez, D.; Ruperez, E.; Gil, F.J. Biofunctionalization strategies on tantalum-based materials for osseointegrative applications. J.Mater. Sci. Mater. Med. 2015, 26: 109. DOI 10.1007/s10856-015-5445-z.
90. Fraioli, R.; Rechenmacher, F.; Neubauer, S.; Manero, J.M.; Gil, J.; Kessler, H.; Mas-Moruno, C. Mimicking bone extracellular matrix: Integrin-binding peptidomimetics enhance osteoblast-like cells adhesion, proliferation, and differentiation on titanium. Colloids Surf. B Biointerfaces 2015, 128: 191–200. https://doi.org/10.1016/j.colsurfb.2014.12.057.
91. Fraoli R , Neubauer S , Rechenmacher F , Bosch BM , Dashnyam K , Kim JH , Perez RA , Kim HW , Gil FJ , Ginebra MP , Manero JM , Kessler H , Mas-Moruno C . Control of stem cell response and bone growth on biomaterials by fully non-peptidic integrin selective ligands. Biomater Sci. 2019, 26;7(4): 1281-1285. doi: 10.1039/c8bm01466c.
92. Fraioli R, Dashnyam K, Kim JH, Perez RA, Kim HW, Gil J, Ginebra MP, Manero JM, Mas-Moruno C. Surface guidance of stem cell behavior: Chemically tailored co-presentation of integrin-binding peptides stimulates osteogenic differentiation in vitro and bone formation in vivo. Acta Biomater. 2016 Oct 1;43:269-281. doi: 10.1016/j.actbio.2016.07.049. Epub 2016 Jul 29. PMID: 27481289
93. Frost HM. Wolff's Law and bone's structural adaptations to mechanical usage: an overview for clinicians. Angle Orthod. 1994, 64(3): 175-88. Frost HM. Doi: 10.1043/0003-3219(1994)064<0175:WLABSA>2.0.CO;2. PMID: 8060014.
94. De Wild M, Schumacher R, Mayer K et al. Bone regeneration by the osteoconductivity of porous titanium implants manufactured by selective laser melting: a histological and micro computed tomography study in the rabbit. Tissue Eng Part A. 2013, 19 (23-24): 2645-54. doi: 10.1089/ten.TEA.2012.0753. Epub 2013 Sep 19. PMID: 23895118.
95. Pattanayak DK, Fukuda A, Matsushita T et al. Bioactive Ti metal analogous to human cancellous bone: Fabrication by selective laser melting and chemical treatments. Acta Biomater. 2011, 7 (3): 1398-1406. ISSN 1742-7061, https://doi.org/10.1016/j.actbio.2010.09.034.
96. Liu YL, Schoenaers J, Groot K et al. Bone healing in porous implants: a histological and histometrical comparative study on sheep. J mat. sci mat. med. 2000, 11: 711-717. doi: 10.1023/a:1008971611885. PMID: 15348077.
97. Kujala S, Ryhänen J, Danilov A et al. Effect of porosity on the osteointegration and bone ingrowth of a weight-bearing nickel-titanium bone graft substitute. Biomaterials 2003, 24: 4691-4697. doi: 10.1016/s0142-9612(03)00359-4. PMID: 12951012.
98. Takemoto M, Fujibayashi S, Neo M, Suzuki J, Kokubo T, Nakamura T. Mechanical properties and osteoconductivity of porous bioactive titanium. Biomaterials. 2005, 26 (30): 6014-23. doi: 10.1016/j.biomaterials.2005.03.019. PMID: 15885769.
99. Hudak R. Biomedical Engineering – Technical Applications in Medicine. Chapter 2: Porous Titanium by Powder Metallurgy for Biomedical Application: Characterization, Cell Citotoxity and in vivo Tests of Osseointegration. Intech Open; 2012.
100. Bobyn JD, Pilliar RM, Cameron HU, Weatherly GC. The optimum pore size for the fixation of porous-surfaced metal implants by the ingrowth of bone. Clin Orthop Relat Res. 1980, 150: 263-70. PMID: 7428231.
101. Mediaswanti K, Wen C, Ivanova IP et al. A review on bioactive porous metallic biomaterials. J Biomim Biomater Tissue Eng. 2013, 18(1): 104.
102. Moreica B. Pabbruwe, Owen C. Standard, Charles C. Sorrell, C Rolfe Howlett, Bone formation within alumina tubes: effect of calcium, manganese, and chromium dopants, Biomaterials, 2004, 25 (20): 4901-4910, ISSN 0142-9612, https://doi.org/10.1016/j.biomaterials.2004.01.005.
103. Bungo Otsuki, Mitsuru Takemoto, Shunsuke Fujibayashi, Masashi Neo, Tadashi Kokubo, Takashi Nakamura, Pore throat size and connectivity determine bone and tissue ingrowth into porous implants: Three-dimensional micro-CT based structural analyses of porous bioactive titanium implants, Biomaterials, 2006, 27 (35): 5892-5900, ISSN 0142-9612, https://doi.org/10.1016/j.biomaterials.2006.08.013.
104. Lu, J.X., Flautre, B., Anselme, K. et al. Role of interconnections in porous bioceramics on bone recolonization in vitro and in vivo. Journal of Materials Science: Materials in Medicine. 1999, 10: 111–120. https://doi.org/10.1023/A:1008973120918.
105. Manresa C, Bosch M, Manzanares MC, Carvalho P, Echeverría JJ. A new standardized-automatic method for bone-to-implant contact histomorphometric analysis based on backscattered scanning electron microscopy images. Clin Oral Implants Res. 2014, 25 (6): 702-6. doi: 10.1111/clr.12129.
106. Banhart, J. Manufacturing routes for metallic foams. JOM, 2000, 52: 22–27. https://doi.org/10.1007/s11837-000-0062-8.
107. Kim HM, Miyaji F, Kokubo T, Nishiguchi S, Nakamura T. Graded surface structure of bioactive titanium prepared by chemical treatment. J Biomed Mater Res. 1999, 45 (2): 100-7. doi: 10.1002/(sici)1097-4636(199905)45:2<100::aid-jbm4>3.0.co;2-0. PMID: 10397963.
108. Kim , H.M., Miyaji , F., Kokubo , T. et al. Effect of heat treatment on apatite-forming ability of Ti metal induced by alkali treatment. Journal of Materials Science: Materials in Medicine. 1997, 8: 341–347. https://doi.org/10.1023/A:1018524731409.
109. Kim HM, Miyaji F, Kokubo T, Nakamura T. Preparation of bioactive Ti and its alloys via simple chemical surface treatment. J Biomed Mater Res. 1996, 32 (3): 409-17. doi: 10.1002/(SICI)1097-4636(199611)32:3<409::AID-JBM14>3.0.CO;2-B. PMID: 8897146.
110. Lee BH, Do Kim Y, Shin JH, Hwan Lee K. Surface modification by alkali and heat treatments in titanium alloys. J Biomed Mater Res. 2002, 61 (3): 466-73. doi: 10.1002/jbm.10190. PMID: 12115472.

111. S. Fujibayashi, M. Neo, Hyun-Min Kim, T. Kokubo, T. Nakamura, Osteoinduction of porous bioactive titanium metal, Biomaterials. 2004, 25 (3): 443-450, ISSN 0142-9612, https://doi.org/10.1016/S0142-9612(03)00551-9.
112. Taubert A, Mano JF, Rodríguez-Cabello JC. Biomaterials Surface Science. Chapter 12: Bioactive Ceramic and Metallic Surfaces for Bone Engineering. Wiley-VCH. 2013.
113. Morra M. Biochemical modification of titanium surfaces: peptides and ECM proteins. Eur Cell Mater. 2006, 24 (12): 1-15. doi: 10.22203/ecm.v012a01. PMID: 16865661.